Ultacold Atoms in Optical Lattices

J. H. Thywissen

University of Toronto, Canada

(Dated: March 13, 2023)

CONTENTS

I. WHAT IS AN OPTICAL LATTICE?

These notes were prepared for the 2023 ICTP school on ultracold atoms, in Sao Paulo. Their intent is to introduce graduate students to ultracold atoms in optical lattices. As a pedagogical document, no attempt is made to capture the state of the art in research using optical lattices; the reader is instead referred to a number of published reviews for this (Georges and Giamarchi, 2012; Gross and Bloch, 2017; Jessen and Deutsch, 1996; Lewenstein *et al.*, 2012).

Jean Dalibard's lectures at the College de France include a pedagogical set of notes on optical lattices (2013), an historical review of cold atoms (2014), and more. Absent from our discussion are two developing themes: periodically driven optical lattices (Eckardt, 2017) and topological effects.

This introductory section discusses how a periodic potential is made using interference patterns of laser light. Subsequent sections discuss the eigenvalue problem of non-interacting particles in a lattice (§II), how to think of a particle "at" a particular lattice site (§III), the deep-lattice limit (§V), and an introduction to many-body physics in a lattice (§VI).

A. Two traveling waves

The light emitted by a continuous-wave laser is typically collimated into a beam that is 0.5 mm to 5 mm in diameter. Within the intensity envelope of these beams, laser beams can be treated as monochromatic traveling waves of light. At position $\mathbf{r}$ and time t, the electric field of a travelling wave can be written

$$\boldsymbol{E}(\mathbf{r},t) = E_0\hat{\boldsymbol{\epsilon}}\,\exp(i\boldsymbol{k}\cdot\mathbf{r} - i\omega t) \tag{1}$$

where $\boldsymbol{k}$ is the wave vector, $\hat{\boldsymbol{\epsilon}}$ is the polarization unit vector, and E_0 is the peak electric field. We have adopted complex notation, but the electric field is a physical observable and thus must be real-valued! The complex notation is used just for convenience (e.g., to avoid sinusoids), and maps back onto the (observed) electric field as $\boldsymbol{E}_{\rm real} = \mathrm{Re}\{\boldsymbol{E}\}$. In fact, since we will typically assume a monochromatic $e^{-i\omega t}$ time dependence of the field, we will drop this as $\boldsymbol{E} = \tilde{\boldsymbol{E}}e^{-i\omega t}$, from which $\boldsymbol{E}_{\rm real} = \mathrm{Re}\{\tilde{\boldsymbol{E}}e^{-i\omega t}\}$.

The energy density of an electromagnetic wave is $u = \epsilon_0|\boldsymbol{E}_{\rm real}|^2$. This will oscillate on a time scale not visible to ordinary detectors, so it is convenient to take the time average and multiply by c to get units of intensity, power per area: $I(\mathbf{r}) = c\epsilon_0\overline{|\boldsymbol{E}(\mathbf{r},t)|^2}$. Applying this to Eq. 1, we see that each travelling wave has an intensity $I_0 = \frac{1}{2}c\epsilon_0 E_0^2$.

Now, we are ready to construct a one-dimensional optical lattice by forming a standing wave from two equal-intensity overlapping travelling waves:

$$\tilde{\boldsymbol{E}}_{\rm sw}(\mathbf{r}) = E_0\hat{\boldsymbol{\epsilon}}_1 e^{i\boldsymbol{k}_1\cdot\mathbf{r}} + E_0\hat{\boldsymbol{\epsilon}}_2 e^{i\boldsymbol{k}_2\cdot\mathbf{r}}\,. \tag{2}$$

The intensity of the standing wave is

$$I_{\rm sw}(\mathbf{r}) = \underbrace{2I_0}_{\text{incoherent}} + \underbrace{2I_0\,\mathrm{Re}\{\hat{\boldsymbol{\epsilon}}_1\cdot\hat{\boldsymbol{\epsilon}}_2^* e^{i(\boldsymbol{k}_1-\boldsymbol{k}_2)\cdot\mathbf{r}}\}}_{\text{interference}} \tag{3}$$

The first term on the r.h.s. is what would be expected if the power of the consituant travelling waves added incoherently. The second term in Eq. 3 is an interference term. It appears for two beams that are phase-coherent. With sub-10-MHz frequency stability easily achieved in a modern laser, the coherence length ($\ell_{\rm coh} \sim c/\Delta f$) of light is in excess of 10 m. State-of-the art sources are kHz-line-width fibre lasers, so that the coherence lengths are many kilometres. Thus, we will assume for now that the relative phase of any two interfering laser beams is under perfect experimental control.

The only remaining question is one of polarization. Figure 1 gives several possibilities for linearly polarized beams: that $\hat{\boldsymbol{\epsilon}}_1$ and $\hat{\boldsymbol{\epsilon}}_2$ are parallel, or crossed linearly; and that the local magnetic field is parallel or perpendicular to the electric field. The reason the B-field matters is that atoms respond differently to σ and π polarized light, as discussed in Sec. A.2. If $\hat{\boldsymbol{\epsilon}}_1$ and $\hat{\boldsymbol{\epsilon}}_2$ are parallel, then an intensity pattern will develop. The linear polarization of $\tilde{\boldsymbol{E}}_{\rm sw}$ addresses the π matrix element if $\boldsymbol{B}||\boldsymbol{E}$ (right column of Fig. 1) or equal parts σ^+ and σ^- if $\boldsymbol{B}\perp\boldsymbol{E}$ (centre column of Fig. 1). On the other hand, if $\hat{\boldsymbol{\epsilon}}_1$ and $\hat{\boldsymbol{\epsilon}}_2$ are perpendicular, the interference term in Eq. 3 vanishes, and there is no intensity pattern. The local polarization in $\tilde{\boldsymbol{E}}_{\rm sw}$ has a pattern that goes from purely σ^+ to purely σ^- and back again, in one wavelength (left column of Fig. 1).

What response do these standing-wave fields induce for atoms? This depends critically on the *detuning* $\Delta = \omega - \omega_0$ of the light from the resonant transition frequency of the atom ω_0. Typical detunings for OLs are tens to hundreds of nm, in order to minimize Rayleigh scattering, which can cause atom heating or loss. For alkali atoms (^{6}Li ,^{87}Rb , ^{40}K , etc.) that are commonly used ultracold atoms, and in the limit where Δ is much larger than the fine-structure splitting $\Delta_{\rm FS}$, the induced potential in this limit can be written, at low magnetic field (Grimm *et al.*, 2000), as

$$U(\mathbf{r}) \approx \frac{3\pi c^2}{2\omega_0^3}\frac{\Gamma}{\Delta}\left(1 + \frac{1}{3}\mathcal{P}g_F m_F\frac{\Delta_{\rm FS}}{\Delta}\right)I(\mathbf{r})\,, \qquad \text{(intermediate detuning } \Delta_{\rm FS} \lesssim |\Delta| \ll \omega_0) \tag{4}$$

where $\mathcal{P} = \pm 1$ for $\sigma^\pm$ light and $= 0$ for linearly polarized light, g_F is the gyromagnetic ratio of the ground state, m_F is the magnetic quantum number. A beam that has equal parts σ^+ and σ^- creates two potentials, with $\mathcal{P} = +1$

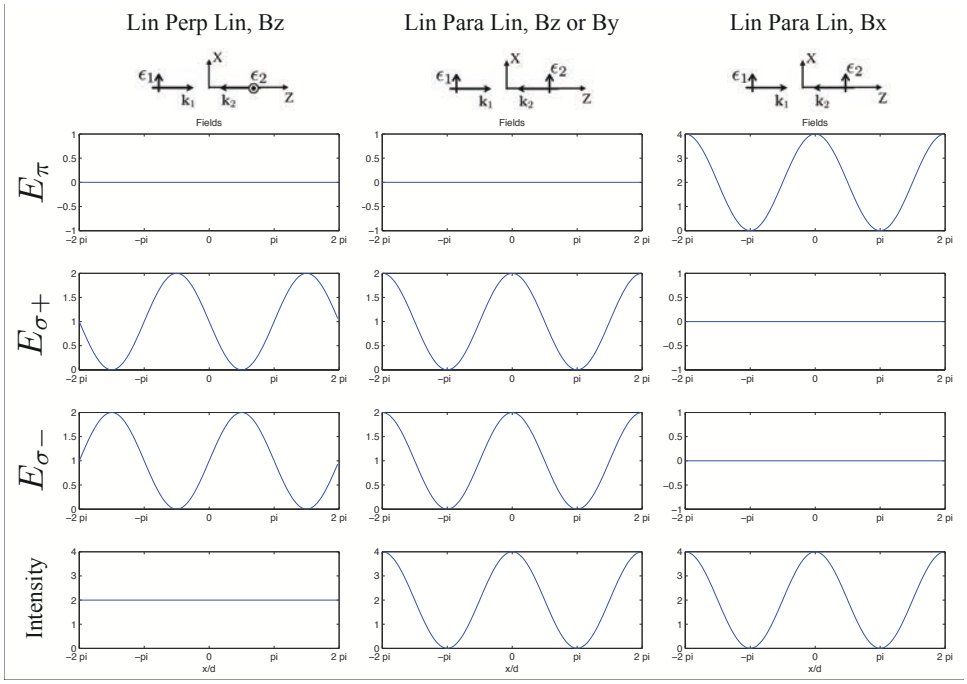

FIG. 1 **Polarizations of standing waves.** Starting with linear polarizations, two equal-intensity counter-propagating travelling waves create a standing wave of intensity or polarization gradient. **Left:** The "lin ⊥ lin" configuration creates no net intensity gradient, but does create an alternating $\sigma+$ / $\sigma-$ polarization standing wave when the magnetic field is oriented in z, parallel to the k vectors of the light. **Centre:** The lin ∥ lin configuration creates a linear polarization and a standing wave in intensity. When the magnetic field is perpendicular to the electric field, that linear polarization is an equal superposition of $\sigma+$ and $\sigma-$ fields. **Right:** When the magnetic field is parallel to the electric field polarization, the lin ∥ lin standing wave is π polarized. Not shown here is a fourth possibility: lin perp lin polarization, like in the left-most column, but a B-field along x or y. In that case, there is neither a polarization gradient nor an intensity gradient.

and -1, such that the polarization effects cancel out. A magnetic potential is only created by an imbalance between σ^+ and σ^- intensities, which can be created with a "lin perp lin" configuration (first column in Fig. 1). Even then, the polarization sensitivity scales as the ratio of the fine-structure splitting Δ_{FS} to the detuning (in alkali atoms). Going forward, we will neglect optically induced magnetic potentials. The force on an atom is just the gradient of this potential — i.e., the dipole force on an atom is proportional to the *gradient in local intensity*, and *independent of the direction of propagation* of the beam.

A contribution to the optical potential not included in Eq. 4 is the counter-rotating term. When magnetic terms are negligible (either because $\mathcal{P} = 0$ or when $|\Delta| \gg \Delta_{\mathrm{FS}}$), the potential is

$$U(\mathbf{r}) \approx \frac{3\pi c^2}{2\omega_0^3}\Big(\underbrace{\frac{\Gamma}{\omega-\omega_0}}_{=\Gamma/\Delta} + \underbrace{\frac{\Gamma}{\omega+\omega_0}}_{\mathrm{counter-rotating}}\Big) I(\mathbf{r}) \qquad \text{(large-detuning limit)} \tag{5}$$

assuming that a single strong dipole transition dominates the static polarizability. In the quasi-static limit $\omega \ll \omega_0$, which describes lattices made by CO_2 lasers at $10\,\mu$m for instance, we see that the counter-rotating term contributes equally to the potential depth, so that Eq. 4 under-estimates the optical potential but as much as a factor of two.

In the true DC limit, electric fields create a static Stark shift:

$$U_{\mathrm{Stark}}(\mathbf{r}) \equiv -\frac{1}{2}\alpha_0 |\boldsymbol{E}|^2(\mathbf{r}) \qquad \text{where} \qquad \alpha_0 = 2\sum_k \frac{\left|\langle 0|\hat{d}\cdot\hat{\boldsymbol{\epsilon}}|k\rangle\right|^2}{E_k - E_0} \tag{6}$$

Extending this treatment to an oscillating electric field, we can replace α_0 by a frequency-dependent polarizability $\alpha(\omega)$. Indeed the first-order perturbative treatment of a time-varying electric field has a similar form to Eq. 6, as shown in App. A. Several characteristics of the static Stark shift carry forward to the effect of a far-detuned laser

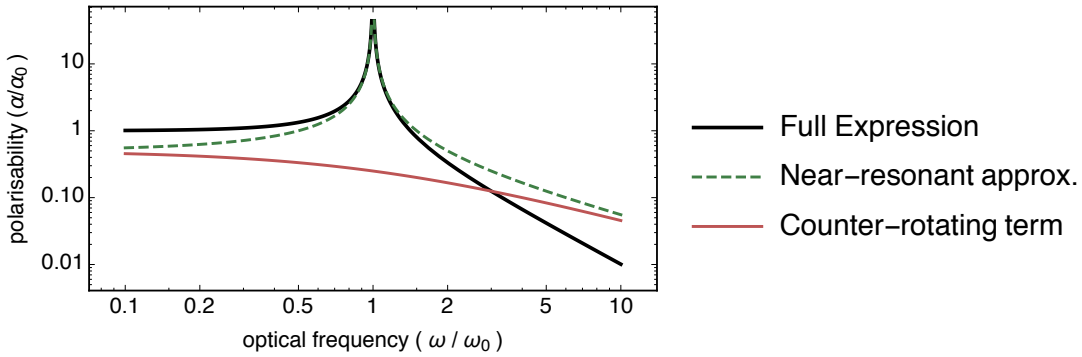

FIG. 2 The polarisability α/α_0 is plotted versus ω/ω_0. The contributions of the resonant enhancement (8) is shown as a dashed green line; and the counter-rotating term is shown as a solid red line. These add to give the solid black line. Notice that the $1/\Delta$ scaling over-estimates polarisability for the ultraviolet limit $\omega \gg \omega_0$, because the counter-rotating term partially counteracts it, resulting in a $1/\Delta^2$ scaling. In the infrared $\omega \ll \omega_0$ limit, the polarisability approaches a constant α_0, and the field can be treated as quasi-electrostatic.

beam on an atom: in both cases, the energetic shift of the ground state is proportional to E^2, and thus proportional to intensity I.

Equation (5) would predict that in the limit $\omega \to 0$, the polarizability $(-2U/E^2)$ approaches

$$\alpha_0 \approx \frac{6\pi c^3 \epsilon_0 \Gamma}{\omega_0^4}\,. \tag{7}$$

Table I compares this to experimentally measured polarizabilities from several alkali metals. We see that at least for the alkali metals, the agreement is better than 5%.

However, the static polarizability $\alpha_0 \approx 3 \times 10^{-39}\,\mathrm{C\,m^2/V}$ of atoms is not promising for static electric fields, since fields greater than 10^5 V/m typically cause electrode discharge. This would limit a Stark shift to $|\Delta E_{\mathrm{Stark}}| \lesssim k_B 2\,\mu\mathrm{K}$, which is only marginally operable for ultracold atoms. Of course, laser light is at a finite frequency ω_L, so offers some resonant enhancement over the static limit. This enhancement factor (again in the far-detuned limit) is clear from Eq. (5):

$$\frac{U_{\mathrm{dip}}}{U_{\mathrm{Stark}}} = \frac{1}{1-(\omega_L/\omega_0)^2} = \frac{1}{1-(\lambda_0/\lambda_L)^2} \tag{8}$$

This is plotted in Fig. 2. A commonly used trapping wavelength is λ_L =1064 nm due to the availability of strong sources at the YAG wavelength. The resonant enhancement factor for the alkali then varies between ∼1.4 (for Na) and ∼2.9 (for Cs).

For far-detuned optical lattices, more significant than this resonant enhancement is the *accessible magnitude* of the electric field (i.e., intensity) that one can achieve using a focused laser beam. For a single-mode Gaussian laser beam

TABLE I Static electric polarizability of alkali atoms. The measured value [ref] is compared to values calculated from (7). Since the strongest dipole line in alkali is split by hyperfine interactions in the excited state, we use $\omega = \bar{\omega}$, where $\bar{\omega}$ is a weighted sum of the fine-structure-split lines: $\bar{\omega} = (1/3)\omega_1 + (2/3)\omega_2$, where ω_1 and ω_2 are the D1 and D2 lines, respectively. Also, $\bar{\Gamma} = (1/3)\Gamma_1 + (2/3)\Gamma_2$, where Γ_1 and Γ_2 are the line widths of the D1 and D2 lines, respectively. The listed wavelengths are $\bar{\lambda} = 2\pi c/\bar{\omega}$.

Element	$\bar{\Gamma}/h$ (MHz)	$\bar{\lambda}$ (nm)	α from Eq. (7) ($10^{-39}\,\mathrm{C\,m^2/V}$)	measured α ($10^{-39}\,\mathrm{C\,m^2/V}$)
Lithium	5.9	671	2.7	2.7
Sodium	9.8	589	2.6	2.6
Potassium	6.0	768	4.7	4.8
Rubidium	6.1	785	5.1	5.3
Cesium	5.0	864	6.3	6.6

propagating along z with a minimum waist at $z = 0$, the intensity is (see (Yariv, 1989), Ch. 6)

$$I(x,y,z) = \frac{2P}{\pi \mathrm{w}^2(z)} \exp\left\{\left[-2\frac{x^2+y^2}{\mathrm{w}^2(z)}\right]\right\} \qquad \text{where} \qquad \mathrm{w}(z) = \mathrm{w}_0\left(1+\frac{z^2}{z_R^2}\right)^{1/2} \quad \text{and} \quad z_R = \pi \mathrm{w}_0^2/\lambda \tag{9}$$

Here P is the optical power (in Watts), $\mathrm{w}(z)$ is the beam waist, w_0 is the minimum beam waist, and z_R is the Rayleigh Range. Notice the easily confused (but commonly used) symbols: w refers to beam radius, while ω_L is an optical frequency. At the focus of the beam, the intensity is

$$I_{\max} = 2P/\pi \mathrm{w}_0^2\,, \tag{10}$$

which for a 5-W beam focused to a waist of 35 μm creates an intensity of $5 \times 10^9\,\mathrm{W/m^2}$. This is an rms electric field of $1.4 \times 10^6\,\mathrm{V/m}$, a very difficult field to create with physical electrodes. A single YAG beam with these parameters creates a traveling-wave potential depth of 680 μK for Potassium, for instance.

Finally, let's put all this back in the context of OLs. Two travelling waves with parallel polarizations and peak intensity I_0 will make a standing-wave intensity pattern

$$I_{\mathrm{sw}}(\mathbf{r}) = 2I_0 + 2I_0\cos(\mathbf{k}_{\mathrm{rel}}\cdot\mathbf{r}) \tag{11}$$

where $\mathbf{k}_{\mathrm{rel}} = \mathbf{k}_1 - \mathbf{k}_2$. For two beams with $\mathbf{k}_{1,2} = \pm k_L\hat{\boldsymbol{x}}$, $\mathbf{k}_{\mathrm{rel}}\cdot\mathbf{r} = 2k_Lx$. Using trig identities, we can also write

$$I_{\mathrm{sw}}(\mathbf{r}) = 4I_0\left(\frac{1}{2}+\frac{1}{2}\cos(2k_Lx)\right) = 4I_0\cos^2(k_Lx) \tag{12}$$

Where did this "factor of 4" come from? One doubling comes from the use of two traveling waves; one doubling comes from the interference effect. The latter does not increase the total power, of course: the spatially averaged intensity is still $2I_0$.

Using Eq. 5, this intensity $4I_0$ translates into a potential depth that we will define as V_L. Whether the potential minimum is at highest or lowest light intensity will depend on Δ; whichever the case, it's mathematically convenient to locate $x = 0$ at the bottom of the potential. So we will typically write

$$\boxed{V(x) = V_L\sin^2(k_Lx) = V_L(1-\cos 2k_Lx) \qquad \text{(1D optical lattice potential)}} \tag{13}$$

The period of this standing wave is $\lambda_L/2$, which is $2\pi/|\mathbf{k}_{\mathrm{rel}}| = \pi/k_L$. It will be useful to rename this as a, the lattice periodicity. For arbitrary angle between laser beams θ,

$$a = \frac{\lambda_L}{2\sin(\theta/2)} \qquad \text{(Lattice period)} \tag{14}$$

which reduces to the minimum length $\lambda_L/2$ for $\theta = \pi$.

B. Interference patterns of multiple traveling waves

So far, we have shown that two traveling waves can create a sinusoidal confining potential. What happens if we add additional beams?

To start with, let's consider three equal-intensity beams. If their polarizations are parallel, then

$$\tilde{\boldsymbol{E}}(\mathbf{r}) = E_0\hat{\boldsymbol{\epsilon}}e^{i\boldsymbol{k}_1\cdot\mathbf{r}} + E_0\hat{\boldsymbol{\epsilon}}e^{i\boldsymbol{k}_2\cdot\mathbf{r}} + E_0\hat{\boldsymbol{\epsilon}}e^{i\boldsymbol{k}_3\cdot\mathbf{r}} \tag{15}$$

and the intensity is

$$I(\mathbf{r}) = I_0\left|e^{i\boldsymbol{k}_1\cdot\mathbf{r}} + e^{i\boldsymbol{k}_2\cdot\mathbf{r}} + e^{i\boldsymbol{k}_3\cdot\mathbf{r}}\right|^2 \tag{16}$$

We will see that the intensity patterns produced are not evident from what seems to be such a simple geometric structure. For three beam at equal angles, we can calculate the intensity pattern in the (x,y) plane with $\boldsymbol{k}_1\cdot\mathbf{r} = k_Lx$, $\boldsymbol{k}_2\cdot\mathbf{r} = k_Lx\cos(2\pi/3) + k_Ly\sin(2\pi/3)$, and $\boldsymbol{k}_3\cdot\mathbf{r} = k_Lx\cos(2\pi/3) - k_Ly\sin(2\pi/3)$. The result is a *honeycomb* or hexagonal pattern. Would you have guessed this?

The situation gets even more complicated with *four* lattice beams in a co-planar arrangement. Now the geometry of the intensity pattern *depends on the relative phase of the beams*. In general, one can show that the geometry of $n+1$ beams in n dimensions is robust to the relative phase, but no more than that. In other words, a tetrahedral configuration of four beams in three dimensions creates a predictable pattern; but the geometry of the interference pattern of five or more beams depends on phase.

A common "trick" used by experimentalists is to wash out interference patterns by using *slightly different optical frequencies* for each 1D standing wave. Frequencies that are offset by tens of MHz (where 1 MHz $= 10^6$ cycles per second $= 2\pi \times 10^6\,\mathrm{s}^{-1}$) will not substantially change the period of the standing waves, since ω_L is typically in the $10^{14}\,\mathrm{s}^{-1}$ regime. However, the interference terms will "walk" at a rate that is too fast for the atoms to follow[1]. A related approach is to use polarizations of standing waves that are mutually orthogonal. In either case, one can create a 2D potential that is

$$V(\mathbf{r}) = V(x) + V(y) = V_{L,x}\sin^2(k_L x) + V_{L,y}\sin^2(k_L y) \qquad \text{(2D square lattice potential)} \tag{17}$$

which is a separable potential with a square structure. Extending to three pairs of beams, for which cross-interferences have been eliminated, we can create

$$\begin{aligned} V(\mathbf{r}) &= V(x) + V(y) + V(z) = V_{L,x}\sin^2(k_L x) + V_{L,y}\sin^2(k_L y) + V_{L,z}\sin^2(k_L z) \qquad \text{(3D cubic lattice potential)} \\ &= V_L\big(3 - \cos(2k_L x) - \cos(2k_L y) - \cos(2k_L z)\big) \quad \text{in the isotropic case} \end{aligned} \tag{18}$$

which is a separable potential with a simple cubic structure. Due to its experimental and theoretical simplicity, this is the "default" OL potential for ultracold atoms, used in the vast majority of labs. Natural crystals do not have the same bias: simple cubic crystals are rare. The second line of Eq. 18 emphasizes that V_L is not the peak depth, but the modulation depth of each individual lattice.

Even without cross-interference patterns, multi-beam lattices can make surprising patterns. Consider laying two potentials like Eq. 17 on top of each other at an angle of $\pi/4$. If all pairs have equal intensity, then the potential is

$$V(\mathbf{r}) = V_L\sin^2(k_L x) + V_L\sin^2(k_L y) + V_L\sin^2(k_L(x+y)/\sqrt{2}) + V_L\sin^2(k_L(x-y)/\sqrt{2}) \tag{19}$$

It turns out that this *is not a periodic potential*! Although it has long-range order, there is no unit cell. Such a potential is called a *quasi-crystal*. Famously, and incorrectly, Linus Pauling said, "there is no such thing as quasi-crystals, only quasi-scientists." Years later, Shectman won a Nobel for his work on quasi-crystals. In 2D, the only possible crystalline orders are rectangular (of which cubic is a special case), centered rectangular, hexagonal, and oblique (of which triangular is a special case). All of them can be made by optical lattices, but only the square lattice has been well explored.

II. BAND STRUCTURE

The treatment of a non-interacting particles in a periodic potential is familiar to anyone who has studied solid state physics. "Band structure" is the starting point for understanding electronic properties of metals and semiconductors. The new perspective offered by cold atom are that the particles might have bosonic statistics (unlike electrons), and eigenstates of the problem can now be understood as atoms dressed by photons. There are also some simplifications: the crystal is completely rigid, since single atoms have negligible back-action on the standing waves, so there are no lattice phonons. Also, the spacing between lattice sites far exceeds the range of inter-particle potentials, at least of dipole-dipole interaction are weak. We shall discuss interactions in §VI; in this section and the next, we focus on the non-interacting problem.

The essence of the problem is the Hamiltonian

$$\hat{H} = \frac{\hat{\boldsymbol{p}}^2}{2m} + V(\hat{\boldsymbol{r}}) \tag{20}$$

where $V(\mathbf{r})$ is the single-particle lattice potential. We will ignore the usual confining potential present in most cold-atom experiments; for a treatment of this, see (Rey *et al.*, 2005), and references therein. For simplicity we treat only

[1] In the limit of deep lattices, the time scale of motional response of a single atom is set by the band gap, $\sim \hbar/\sqrt{E_R V_L}$, which for typical atomic mass and lattice configurations is tens of microseconds. Washing out interference between optical beams is safely accomplished with a $\sim 10^2$ MHz frequency difference, such that the optical pattern walks through a full period on the nanosecond scale.

the 1D sinusoidal problem in these notes, i.e.,

$$\hat{H} = \frac{\hat{p}_x^2}{2m} + V_L \sin^2(k_L \hat{x}) \tag{21}$$

and refer the reading to numerous solid-state physics textbooks for a systematic treatment of three-dimensional band structure.

A. Symmetry of the eigenstates: quasi-momentum

A periodic potential breaks the continuous translational symmetry that is present in free space. Noether's Theorem states that for every continuous symmetry, there is a conserved quantity. For the continuous translational symmetry, it is *momentum* that is conserved, even in a many-body system. For instance, if two particles collide in free space, they can exchange momentum, but the total momentum of the two particles is the same before and after the collision.

The optical lattice ruins all this and more: $V(\mathbf{r})$ is not translationally invariant, so momentum is not conserved. Seen another way: momentum can be transferred between the light and matter, so the atoms' momentum is not conserved. Furthermore, the lattice potential provides a fixed reference frame that destroys Galilean invariance: we can always compare the speed of an atom to the (stationary) lattice potential, which now defines a natural choice for $v = 0$.

However, a periodic potential does have a *discrete translational symmetry*. Shifting the potential by one spatial period returns us to the original scenario. A natural question to ask is whether there is some conserved quantity that is the complement of this newly restricted symmetry. Bloch (1929) and Floquet (1883) found that indeed, there is a new quantity, "crystal momentum" or "quasi-momentum", which characterizes the eigenstates $|\Phi\rangle$ of Eq. 20. We will first show the structure of the solution for the 1D case, and then return to the 3D case.

The translation operator $\hat{T}_a$ is defined by

$$\hat{T}_a |x\rangle = |x + a\rangle \quad \text{such that} \quad \hat{T}_a \Phi(x) = \langle x | \hat{T}_a | \Phi \rangle = \langle x - a | \Phi \rangle = \Phi(x - a_L)\,. \tag{22}$$

Since momentum operator $\hat{p}_x$ is (also defined as) the generator of translations in x, we can write

$$\hat{T}_a = e^{-ia\hat{p}_x/\hbar}\,. \qquad \text{(Spatial translation operator)} \tag{23}$$

Our 1D Hamiltonian $\hat{H}_x = \hat{p}_x^2/2m + V(\hat{x})$ commutes with $\hat{T}_a$ when a is the period of the lattice because $V(x) = V(x \pm a)$, and $\hat{p}_x$ commutes with $\hat{T}_a$ for any a. Thus, when looking for the eigenvalues of $\hat{H}_x$, we know they should also be eigenstates of $\hat{T}_a$.

First, let's show that $\hat{T}_a$ is a unitary operator, whose inverse is its hermetian conjugate:

$$\hat{T}_a^{-1} = (e^{-ia\hat{p}_x/\hbar})^{-1} = e^{+ia\hat{p}_x/\hbar} = \hat{T}_a^\dagger \tag{24}$$

Hermetian operators have the nice property that their eigenvalues have unity modulus[2], we can write them as $\lambda = e^{i\theta}$, and label the eigenstates with θ; or, we could choose to write $\lambda = e^{-iqa_L}$, where a_L is fixed (the period of the lattice), and associate each eigenstate with a new variable q, a wave number that must have units of inverse length. Our eigenstates are now $|q\rangle$, with eigenvalues of $\hat{T}_a$ that are $\hat{T}_a |q\rangle = e^{-iqa} |q\rangle$.

Without loss of generality, we can write these eigenstates in the form

$$\langle x|q\rangle = \Phi_q(x) = e^{iqx} u_q(x) \qquad \text{where} \quad u_q(x - a) = u_q(x) \qquad \text{(Bloch waves)} \tag{25}$$

where we still need to find the form of the periodic function $u_q(x)$. Note that *the full function $\Phi_q(x)$ is not periodic*: there is a phase difference e^{iqa} between between one period and the next. This reminds of us a plane wave, whose phase also evolves by e^{ika} between any two points a apart, and thus q is called the *quasi-momentum*[3].

What is the relationship between quasi-momentum and true momentum? The relationship is not simple. $\Phi_q(x)$ is a plane wave times a spatial modulation $u_q(x)$ that is periodic in x, and whose momentum components are non-trivial:

$$u_q(x) = \sum_j c_j^q e^{2ijk_L x} \tag{26}$$

for integer j and (recall) $k_L = \pi/a$. The Fourier-series representation of u_q ensures its periodicity: replacing x by $x + a$ modifies the phase factor to be $e^{2ijk_L a} = e^{ij2\pi} = 1$.

---

[2] Proof of this is as follows. Let's take an eigenstate ϕ of operator $\hat{U}$, with eigenvalue λ, i.e., $\hat{U}\phi = \lambda\phi$. The modulus $|\lambda\phi|^2 = |\hat{U}\phi|^2 = \phi^* \hat{U}^\dagger \hat{U} \phi$. But for unity operators, $\hat{U}^\dagger \hat{U} = 1$, so $|\lambda\phi|^2 = |\phi|^2$. However, this can only be true if $|\lambda|^2 = 1$. QED.

[3] No relation to the quasi-crystals discussed in §I.B

B. The eigenvalue problem

Solving the eigenvalue problem for each q entails finding the $\{c_j^q\}$. Then,

$$\Phi_q(x) = \sum_j c_j^q e^{i(q+2jk_L)x} \qquad \text{or} \qquad |q\rangle = \sum_j c_j^q \, |p = q + 2jk_L\rangle \tag{27}$$

We see that each quasi-momentum state consists of a *comb of real momenta* q, $q \pm 2k_L$, $q \pm 4k_L$, etc. whose spacing is $2\hbar k_L$, i.e., the momenta of two photons at the wavelength of the lattice.

The eigenstates and precise eigenvalues of the problem can be found by substituting Eq. 27 into Eq. 20. We have already discussed why these states are labelled $|q\rangle$; the remaining unknown function is $u_q(x)$, described by a series of coefficients c_j. It is convenient to rescale everything in the problem by the energy scale $E_R = \hbar^2 k_L^2/2m$, length a_L, and wave vector $k_L = \pi/a_L$. The eigenvalue problem now distills down to a single matrix equation

$$\sum_{\ell'} [H_q]_{\ell\ell'} c_{\ell'} = \frac{E_q}{E_R} c_\ell \tag{28}$$

where

$$[H_q]_{\ell\ell'} = \big((\frac{qa_L}{\pi} + 2\ell)^2 + \frac{s}{2}\big)\delta_{\ell,\ell'} - \frac{s}{4}\delta_{\ell,\ell'-1} - \frac{s}{4}\delta_{\ell,\ell'+1} \tag{29}$$

which is a tri-diagonal matrix that looks like

$$H_q \to \begin{pmatrix} (qa_L/\pi + 4)^2 & -s/4 & 0 & 0 & 0 \\ -s/4 & (qa_L/\pi + 2)^2 & -s/4 & 0 & 0 \\ 0 & -s/4 & (qa_L/\pi)^2 & -s/4 & 0 \\ 0 & 0 & -s/4 & (qa_L/\pi - 2)^2 & -s/4 \\ 0 & 0 & 0 & -s/4 & (qa_L/\pi - 4)^2 \end{pmatrix} \tag{30}$$

where we have only written out the central 5x5 elements of this infinite matrix. The eigenvectors are column vectors of the coefficients $\{c_\ell\}$. From these, you can assemble the previously unknown function $u(x) = \sum_\ell c_\ell \exp(2i\ell k_L x)$. Note that $\sum |c_\ell|^2 = 1$.

Practically speaking, you will have to truncate this matrix to some $\pm\ell_{\max}$. This can be safely down when $(qa_L/\pi + 2\ell_{\max})^2 \gg s/4$, so that the plane-wave states are unaffected by Bragg scattering of the lattice. In practice, $\ell_{\max} = 3$ can work for weak lattices, and $\ell_{\max} = 10$ can work for deep lattices. This matrix approach is general, and can be generalized to complex and multi-dimensional lattice structure.

For the 1D sinusoidal potential, it turns out that this eigenvalue problem can be mapped to a set of analytic functions developed by Mathieu, while studying vibrational modes of drumheads. The Mathieu equation is

$$\frac{d^2}{dz^2} y + [\varepsilon - 2\mathtt{v}\cos(2z)]\, y = 0 \tag{31}$$

and yields periodic solutions of even parity when $\varepsilon = \mathtt{a}(r, \mathtt{v})$, and odd parity when $\varepsilon = \mathtt{b}(r, \mathtt{v})$, where r is a "characteristic exponent" that maps onto the quasi-momentum in our problem: $r \to q/k_L = \pi q/a_L$. The solutions to this differential equation are special functions: "cosine-elliptic" $y = \mathrm{ce}(r, \mathtt{v}, z)$ and "sine-elliptic" $y = \mathrm{se}(r, \mathtt{v}, z)$, respectively. For $\mathtt{v} = 0$, $\mathrm{ce} \to \cos(\sqrt{\varepsilon} z)$ and $\mathrm{se} \to \sin(\sqrt{\varepsilon} z)$.

Mapping Eq. 31 to Eq. 21 with $\langle x|\, \hat{H}\, |\psi\rangle = \langle x|\, E\, |\psi\rangle$ uses $\mathtt{v} \to -V_L/4E_R$ and $\varepsilon \to E/E_R - V_L/2E_R$. We are left with two continua of possible solutions:

$$\begin{aligned} &\Phi_q(x) = \mathrm{ce}(q/k_L, \mathtt{v}, k_L x) \quad \text{with} \quad E_q = \mathtt{a}(q/k_L, \mathtt{v})E_R + V_L/2 \qquad \text{(even parity)} \\ &\Phi_q(x) = \mathrm{se}(q/k_L, \mathtt{v}, k_L x) \quad \text{with} \quad E_q = \mathtt{b}(q/k_L, \mathtt{v})E_R + V_L/2 \qquad \text{(odd parity)} \end{aligned} \tag{32}$$

where we have not specified the normalization. That there are two solutions to this equation poses a problem in a sense: are there two eigenvalues for each q? In fact, $\mathtt{a}$ and $\mathtt{b}$ are different only for *integer* r, i.e., $q = n\, k_L$. As we shall see in the next section, these critical points are *Bragg planes* that correspond to *gaps in the energy spectrum*, where for a single q, there are two possible eigenstates. The nth energy gap (between those eigenstates) is $|\mathtt{a}(n, \mathtt{v}) - \mathtt{b}(n, \mathtt{v})|E_R$. Apart from those gaps, $\mathtt{a}(r, \mathtt{v}) = \mathtt{b}(r, \mathtt{v})$, however we still need to choose between the two parity of solutions (which are different even for non-integer r). As we discuss in the next section, this is resolved by partitioning the eigenspectrum into *bands*, enumerated with positive integers n. The band index n, shared by all quasi-momenta in the band, is the number of Bragg planes (and thus gaps) crossed in going from $q = 0$ to the q in that band. Once the band is established, one can choose the correct solution: odd n have odd-parity $\Phi_q(x)$, and even n have even-parity $\Phi_q(x)$.

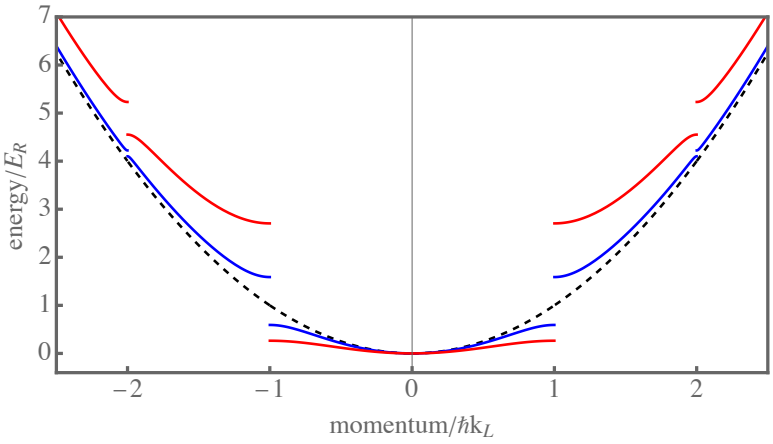

FIG. 3 Opening of band gaps. A free-particle dispersion relation ($V_L = 0$) is shown as a black dashed line. The eigenvalues of H_q are shown for $V_L = 2E_R$ (blue solid line) and for $V_L = 5E_R$ (red solid line). Here we have offset the curves such that all energies to overlap at $q = 0$.

C. Bragg scattering and band gaps

Before proceeding further to discuss the solutions of the eigenvalue problem, let's pause to consider the physical picture. Why does the $|q\rangle$ state in Eq. 27 consist of a comb of momenta spaced by *two* photon momenta?

The explanation comes from considering the wave-like properties of matter: the structure of $|q\rangle$ reflects the *diffraction of matter waves from a periodic potential*. nth-order Bragg scattering occurs for a wave of wavelength λ interacting with a periodic structure of period a, when the (equal) incident and reflected angle θ satisfy

$$2a \sin\theta = n\lambda \,. \tag{33}$$

In our case, the wave is a de-Broglie wave with $\lambda \to \lambda_{\rm dB} = h/|p_x|$ and retro-reflection in the standing wave has $\theta = \pi/2$, so that $\sin\theta = 1$. This gives $|p_x| = n\frac{h}{2a} = nh/(2\pi/k_L) = n\hbar k_L$ since $a = \pi/k_L$. Thus

$$p_x = \pm n\hbar k_L \tag{34}$$

are the resonant momenta at which atoms Bragg scatter off of the optical lattice.

When Bragg scattering does occur, both momentum and energy are conserved. The first-order process is as follows: an atom moving at momentum $p_{x,i} > 0$

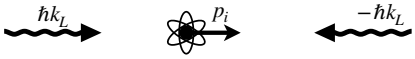

is converted to a final momentum $p_{x,i} - 2\hbar k_L$,

which conserves momentum because the number of photons moving in the $-x$ direction decreases by one, and the number of photons moving in the $+x$ direction increases by one. *The optical field absorbs the momentum of the scattered atom.* If all photons have the same frequency, the energy of the light field is unchanged, so the energy of the atom must also be unchanged; this can only happen when $p_{x,f}^2 = p_{x,i}^2$, i.e., $p_{x,f} = -p_{x,i}$. Putting energy and momentum conservation together, we find again the condition in Eq. 34 for $n = 1$.

Bragg scattering is a two-photon process[4]. Two-photon coupling generally occurs at a strength $\hbar\Omega_{\rm Ram}$ that is given by the 2-photon (or Raman) Rabi frequency ,

$$\Omega_{\rm Ram} = \frac{\Omega_1\Omega_2}{2\Delta} \,, \tag{35}$$

[4] Note that this is not the same as a time-ordered sequence of two single-photon processes. Bragg scattering is also fully coherent, and it does not involve spontaneous emission.

where Ω_1 and Ω_2 are single-photon Rabi frequencies, given by Eq. A9. In this case, these single-photon Rabi frequencies are (separately) based on the electric field for a travelling-wave beam and the electric dipole moment of the ground-to-excited-state transition. The standing-wave lattice potential is *also* created from a second-order process in the electric field, $V_L = \hbar\Omega_L^2/4\Delta$, but where Ω_L comes from the *total* electric field, including all the interference terms discussed in §I.A; whereas $\Omega_{\rm Ram}$, Ω_1, and Ω_2 are spatially constant. Thus $\Omega_{1,2} = \Omega_L/2$, and $\Omega_{\rm Ram} = V_L/2\hbar$. `Check factors.`

Bragg scattering is the process in which a two-photon (or $2n$-photon) transition changes the momentum of the atom. Wave-function overlap requires momentum conservation, such that Bragg processes can only be driven by the part of the optical field that provides the needed $2n\hbar k$. We can find what is needed for a $\pm 2\hbar k_L$ change directly in the standing-wave potential, by writing it as

$$V_L \sin^2(k_L x) = \frac{V_L}{2} - \frac{V_L}{4} e^{2ik_L x} - \frac{V_L}{4} e^{-2ik_L x} \,. \tag{36}$$

We see that only the $V_L/4$ components could couple momentum states that differ by $2\hbar k_L$; the spatially uniform $V_L/2$ provides an energy offset to eigenstates. Since coupling strengths are always $\pm\hbar\Omega_{\rm Rabi}/2$, we read off the first-order Bragg scattering Rabi frequency as

$$\Omega_{B,1} = \frac{-V_L}{2\hbar} = \Omega_{\rm Ram} \,. \tag{37}$$

Higher-order Bragg scattering also requires considering the detunings of intermediate states. Going from $-2\hbar k_L$ to $+2\hbar k_L$ is a second-order process (so proportional to $(-V_L/2)^2$), through the intermediate virtual state $|p = 0\rangle$, whose detuning is $4E_R$. We'd thus expect the $\hbar\Omega_{B,2}$ to be $(V_L/2)^2/(4E_R) = 2^{-4}V_L^2/E_R$. Indeed, more careful treatments(Giltner *et al.*, 1995; Müller *et al.*, 2008) find that

$$\Omega_{B,n} = \frac{\Omega_{\rm Ram}^n}{(8E_R/\hbar)^{n-1}((n-1)!)^2} = \frac{(-V_L/2\hbar)^n}{(8E_R/\hbar)^{n-1}((n-1)!)^2} \tag{38}$$

is the Rabi frequency for nth-order Bragg scattering, which couples $p_{x,i}$ to $p_{x,i} \pm 2n\hbar k_L$, through a $2n$-photon coherent process. The first-order $\hbar\Omega_{B,1} = V_L/2$, the second-order process is $\hbar\Omega_{B,2} = V_L^2/32E_R$, etc.

Let's now discuss how Bragg scattering breaks the energy continuum of a free-particle dispersion relation into distinct energetic bands. The eigenvalues of Eq. 20 with $V(x) = 0$ are simply $E = p_x^2/2m$, shown as a dashed line in Fig. 3. The addition of a weak lattice will shift this curve by $V_L/2$ (see Eq. 36), and leave most of the curve unaffected, expect for places where the resonance condition Eq. 34 is met. The strongest modification occurs for the first-order Bragg resonance, so let's consider that first.

A simple Hamiltonian for this is

$$H_{B,1} = \begin{pmatrix} p_i^2/2m & \hbar\Omega_{B,1}/2 \\ \hbar\Omega_{B,1}/2 & p_f^2/2m \end{pmatrix} = \begin{pmatrix} E_R & -V_L/4 \\ -V_L/4 & E_R \end{pmatrix} \tag{39}$$

This is easy to diagonalize: $E = E_R \pm \hbar\Omega_{B,1}/2$, such that an *energy gap* opens up with a width $\hbar|\Omega_{B,1}| = V_L/2$ (see $\pm\hbar k_L$ in Fig. 3). This is a radical change to the structure of allowed energy eigenstates: none may exist with this gap. We call the continuum of q and energies leading up to this first gap the *lowest band*, and the continuum above this gap the *first excited band*. We will assign these bands the indices $n = 0$ and $n = 1$, respectively.

A similar phenomenon happens at $p = -2\hbar k_L$ and $p = +2\hbar k_L$. These two states are coupled through second-order Bragg scattering. Since the $p = 0$ virtual state is involved in this second-order process, we can find the gap by diagonalizing

$$H_{B,2} = \begin{pmatrix} p_i^2/2m & -V_L/4 & 0 \\ -V_L/4 & 0 & -V_L/4 \\ 0 & -V_L/4 & p_f^2/2m \end{pmatrix} = \begin{pmatrix} 4E_R & -V_L/4 & 0 \\ -V_L/4 & 0 & -V_L/4 \\ 0 & -V_L/4 & 4E_R \end{pmatrix} \tag{40}$$

or by using Eq. 38, which has already eliminated the off-resonant states:

$$H_{B,2} \to \begin{pmatrix} p_i^2/2m & \hbar\Omega_{B,2}/2 \\ \hbar\Omega_{B,2}/2 & p_f^2/2m \end{pmatrix} \tag{41}$$

In either case, in the limit $V_L \ll E_R$, we find eigenvalues near $4E_R$ that are split by $V_L^2/(32E_R)$, i.e., at $\pm\hbar\Omega_{B,2}/2$ given by Eq. 38. For a weak optical lattice, this second gap is smaller than the first gap: see $\pm 2\hbar k_L$ in Fig. 3. However

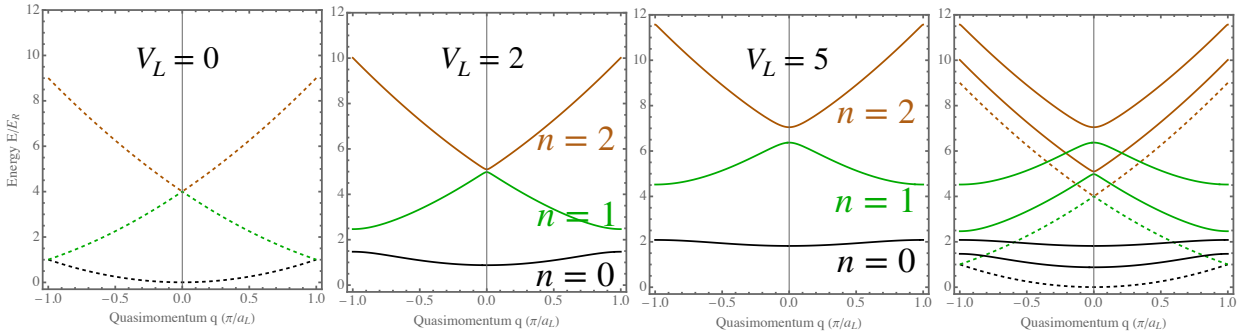

FIG. 4 **Band structure** The same band structure plotted in Fig. 3 is shown here again, but for the "reduced zone scheme", where q goes only from $-\hbar k_L = \pi/a_L$ to $+\hbar k_L$, but now $E_q^{(n)}$ also contains a band index. The first three bands are labelled; diagrams are shown for $V_L = 0$, $V_L = 2$, and $V_L = 5$. Unlike in Fig. 3, we have not shifted energy curves to overlap at $q = 0$.

the same *structural* change occurs in the eigenspectrum, i.e., a *first excited band* of continuous energies below $4E_R$ is gapped from a *second band* of continuous energies above it. This is the dividing point between the $n = 1$ and $n = 2$ bands.

In sum, we find that coherent coupling of atomic momentum states breaks the continuum of $p^2/2m$ free-particle energies into an infinite number of bands. The gaps between the bands are proportional to atom-photon coupling strengths required to couple the $\pm 2n\hbar k_L$ momenta at the edges of the bands. In the next section, we discuss the structure of these bands.

D. Band structure

A property of the infinite-dimensional matrix H_q is that the same eigenspectrum results when considering q or any $q + 2n\pi/a$, for integer n. We can see this by examining the on-diagonal elements of Eq. 30: adding $2\pi/a_L$ to q simply shifts those entries down by one diagonal step. But since this is an infinite matrix, this leaves the Hamiltonian unchanged. A similar property applies to the eigenstates: notice that the eigenvalues of $\hat{T}_{a_L}$, $\lambda = e^{-iqa_L}$, are unchanged for $q \to q + 2\pi/a_L$. The eigenstates $|q\rangle$ are always arbitrary up to an overall phase, but clearly the eigenvalue problem is only distinct within a range $q = (-\pi/a_L, +\pi, a_L)$. For this reason, the eigenspectrum is only shown for q up to $\pm\pi/a_L$. This is called the "folded band" representation, and shown in Fig. 4.

Notice that the energies shown are identical for q and $-q$. This is due to time-reversal symmetry of the Hamiltonian. Time reversal changes $\hat{\boldsymbol{p}}$ to $-\hat{\boldsymbol{p}}$, but leaves $\hat{\boldsymbol{r}}$ unchanged. Since there is no magnetic field under consideration (which would have contributed a $\hat{\boldsymbol{p}} \cdot \boldsymbol{A}$ term), $\hat{H}$ is quadratic in $\hat{\boldsymbol{p}}$ and therefore unchanged. This carries through to quasimomentum, as $E(-\boldsymbol{q}) = E(\boldsymbol{q})$. For this reason, applying a "modulo 2π" to qa_L when plotting the $E(q)$ spectrum makes it looks as if the energy diagram were "folded"; hence the name.

At each q, the solutions to Eq. 28 can be sorted by increasing energy, and labelled with the *band index* $n = 0, 1, 2, \ldots$. We will refer to them as $E_q^{(n)}$. Figure 5 shows the range of solutions within each band as a function of depth. The range of energies within each band is the *band width* W_n:

$$W_n = \max_q E_q^{(n)} - \min_q E_q^{(n)} \tag{42}$$

We will show below that for deep lattices, W_n is proportional to the site-to-site tunnelling strength. The gaps between bands are BG_n, defined as

$$\mathrm{BG}_{n\to n+1} = \min_q E_q^{(n+1)} - \max_q E_q^{(n)} \tag{43}$$

We note that for more complex lattice structure than the one considered here, full band gaps may not exist between bands.

A feature of Fig. 4 is that the dispersion is flat at the edges of each band, i.e., $dE^{(n)}/dq = 0$. This feature arises from the nature of the avoided crossing, as follows. As discussed in §II.C, nth-order Bragg resonances occur near resonant momenta $q_n = nk_L$. Consider a small displacement $\delta_k = q - q_n$: here $q_i = q_n + \delta_k$ is coupled to $q_f = q_i - 2q_n = \delta_k - q_n$.

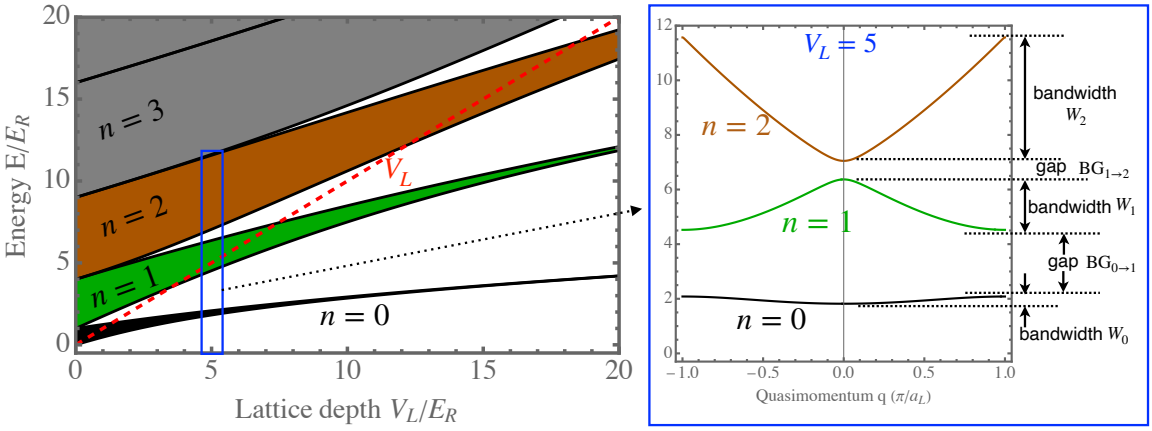

FIG. 5 **Bandwidths and band gaps.** The range of solutions $\{E_q^{(n)}\}$ is shown for a range of lattice depths. At one particular depth, a panel from Fig. 4 is repeated, but this time labelling the widths W_0, W_1, and W_2, as well as the first two gaps, $\mathrm{BG}_{0\to1}$ and $\mathrm{BG}_{1\to2}$. For comparison, the lattice depth is shown (red dashed line). We see that gaps appear even for energies above V_L.

The effective Hamiltonian is

$$H \to \begin{pmatrix} \frac{\hbar^2}{2m}(q_n+\delta_k)^2 & \hbar\Omega_{B,n}/2 \\ \hbar\Omega_{B,n}/2 & \frac{\hbar^2}{2m}(-q_n+\delta_k)^2 \end{pmatrix} \approx n^2 E_R + \begin{pmatrix} 2nE_R(\delta_k/k_L)^2 & \hbar\Omega_{B,n}/2 \\ \hbar\Omega_{B,n}/2 & -2nE_R(\delta_k/k_L)^2 \end{pmatrix} \tag{44}$$

where we have dropped terms of order δ_k^2. Diagonalizing this Hamiltonian, we find that for small δ_k,

$$E_q^{(n)} \approx n^2 E_R - \frac{\hbar\Omega_{B,n}}{2}\left(1+\frac{1}{2}(\frac{2n\hbar k_L}{m\Omega_{B,n}})^2\delta_k^2\right) \quad \text{and} \quad E_q^{(n+1)} \approx n^2 E_R + \frac{\hbar\Omega_{B,n}}{2}\left(1+\frac{1}{2}(\frac{2n\hbar k_L}{m\Omega_{B,n}})^2\delta_k^2\right) \tag{45}$$

This shows that energy is quadratic in $\delta_k = q - q_n$ near the band edge, and thus that $dE^{(n)}/dq = 0$ at $\delta_k = 0$.

E. Bloch states

Having solved the eigenvalue problem numerically, we can calculate both $u_q^{(n)}(x)$ and $\Phi_{n,q}(x)$. As mentioned before, the overall phase of each eigenfunction can be chosen freely. A standard convention is to choose $\Phi_{n,q}(x=0)$ to be real and positive for even n, and $d\Phi_{n,q}(x)/dx|_{x=0}$ to be real and positive for odd n.

The simplest example of a Bloch state is the $q=0$ state in the lowest band:

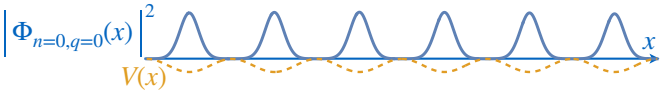

here shown for $V_L = 20E_R$. We see that the amplitude of $|\Phi_{n,q}|^2$ is maximal at the bottom of the lattice potential (which has been shifted downwards for clarity). For the $n=1$ band, the on-site function aquires a node:

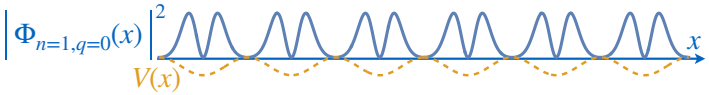

and for the $n=2$ band, two nodes:

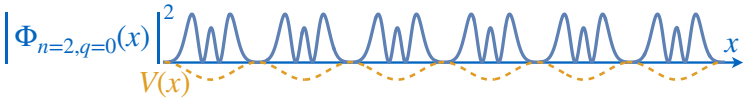

here shown for $V_L = 50E_R$. We will see in §III.D that in the limit of a deep lattice, the wave function at each site approaches a harmonic oscillator. Already, these Bloch wavefunctions resemble the $n = \{0,1,2\}$ harmonic oscillator eigenstates.

As eigenstates of a Hermetian operator, the Bloch states form an orthogonal basis:

$$\langle n,q|n',q'\rangle = \delta_{n,n'}\delta(q-q') \tag{46}$$

or, inserting $1 = \int |x\rangle \langle x|$, an equivalent relation in the spatial domain is:

$$\int_{-\infty}^{+\infty} dx\, \Phi^*_{n,q}(x)\Phi_{n',q'}(x) = \delta_{n,n'}\delta(q-q') \tag{47}$$

In this way Bloch states behave much like momentum eigenstates. For the examples of $q = 0$ states given above, the orthogonality of different bands is already suggested in the nodal structure of the on-site wavefunction.

For different q states within the same band, it is instead the long-range structure that shows the character of the eigenvector. We see this in the following sequence for $n = 0$ band Bloch functions (shown for $V_L = 50E_R$) at variable q:

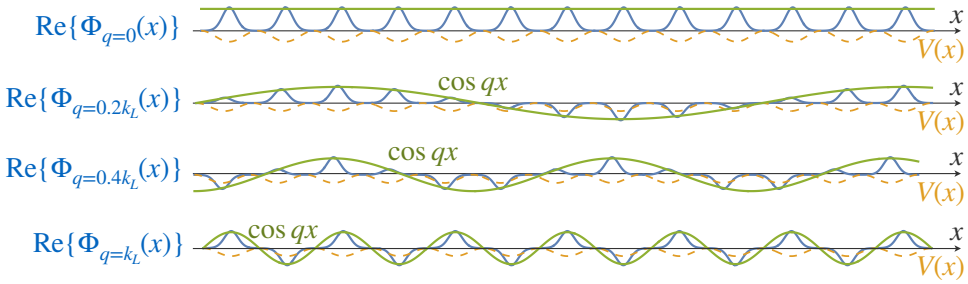

Note that negative q solutions are identical to positive q solutions for parity-symmetric lattices ($V(-x) = V(x)$), so we only show examples of $q \geq 0$. In each plot, $\mathrm{Re}\{\Phi_q\}$ is compared to $\cos qx$, which is the real part of the e^{iqx} prefactor from Eq. 25. At the largest quasi-momentum in the lowest band, $q = k_L = \pi/a_L$, the period of the wave function is $2a_L$, which may at first seem strange. (Did you expect half this period, a_L?) Going back to smaller lattice depths lets us see why this is natural. As $V_L \to 0$, the Bloch function becomes a plane-wave function. For example, at $V_L = E_R$,

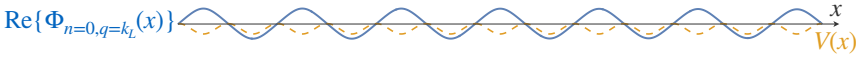

In this limit, a plane wave at the maximum $q = k_L$ is $\Phi_{q=k_L} \to \exp(ik_L x)$. The period of this function is $2\pi/k_L$, which is $\lambda_L = 2a_L$. Just across the band gap, one finds a wave function with the same period, but offset phase,

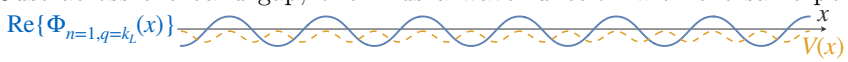

i.e., $\mathrm{Re}\Phi_{n=1,q=k_L} \sim \sin k_L x$ instead of $\mathrm{Re}\Phi_{n=0,q=k_L} \sim \cos k_L x$, so that the two Bloch functions at the avoided crossing (see Eq. 39) are orthogonal.

F. Band mapping

III. LOCALIZATION AND TUNNELLING

Let's now put individual atoms into the modes derived in §II, and try to understand their spatial motion. Of course, an atom in a Bloch state has no dynamics: Bloch state are eigenstates. However initializing particles in delocalized states is not always natural for an experiment. For instance, interactions (discussed in §VI) may localize particles. In this section we show how tunnelling – one of the most iconic quantum phenomona – is already present in band structure.

A. Localization

How do we describe a localized particle in an optical lattice? As a warm-up, let's ask this question without the periodic potential; and then return to a system with band structure.

In an infinite system, the plane-wave eigenstates with $E = \hbar^2k^2/2m$ are $\phi(x) = \exp(ikx)$, neglecting normalization for now. A localized wave function, centred at x_c, has a position-space representation[5]

$$\psi_{x_c}(x) = \langle x|x_c\rangle = \delta(x - x_c) \tag{48}$$

[5] In this section and the next, we will neglect the normalization of wave functions, and restore them in §III.C.

where $\delta(\cdot)$ is the Dirac delta function. In momentum space,

$$\psi_{x_c}(k) = \langle k|x_c\rangle = \exp(-ikx_c) \tag{49}$$

This uses all momentum states: *localization to a single point in position space requires delocalization in momentum space*. We expect this, of course, from the Heisenberg uncertainly principle, which is just a consequence of Fourier relations.

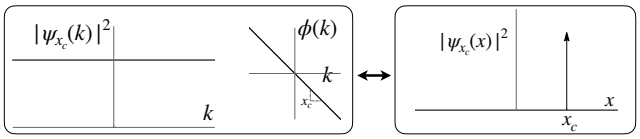

We can summarize this as

$$|x_c\rangle = \int_{k=-\infty}^{k=+\infty} dk\, e^{i\phi(k)}\, |k\rangle \qquad \text{with} \quad \phi(k) = -kx_c \tag{50}$$

The particular phase chosen for each momentum state, $\phi(k) = -kx_c$, is essential to coherently sum to the delta function at x_c.

For a particle in a *single* band of an optical lattice, we don't have all momenta: only q (which for $V_L = 0$, is the same thing as k) between $-\pi/a_L$ and $\pi/a_L = k_L$. Using these, how localized can the state be? What's unclear is which *phases* $\phi(q)$ give the optimal localization. Kohn (Kohn, 1959) showed that the optimal choices can give exponential localization, so long as band gaps exist.

Even though we do not have a band gap for $V_L = 0$, it is illustrative to try to localize a particle with a single-band range of momenta (since the math is particularly simple).

$$|\psi_{x_c}\rangle = \int_{k=-\pi/a_L}^{k=+\pi/a_L} dk\, e^{i\phi(k)}\, |k\rangle \tag{51}$$

If we choose $\phi(k) = 0$, then

$$\langle x|\psi_0\rangle = \psi_0(x) = \frac{2\sin k_L x}{x} = \mathcal{N}\,\mathrm{sinc}(k_L x) \tag{52}$$

where $\mathcal{N}$ is a normalization factor (which we are going to neglect for now). This is a "sinc" function, whose nodes (given by $k_L x = \pm\pi, \pm 2\pi$, etc.) are $\pm a_L$, $\pm 2a_L$, etc. We could displace this wavefunction by choosing $\phi(k) = -kx_c$, which is equivalent to applying the translation operator $\hat{T}(x_c) = e^{-i\hat{p}x_c/\hbar}$, to $|\psi_0\rangle$. Together, this gives

$$|\psi_{x_c}\rangle = \int_{k=-\pi/a_L}^{k=+\pi/a_L} dk\, e^{-ikx_c}\, |k\rangle \tag{53}$$

whose momentum and position representations are as follows:

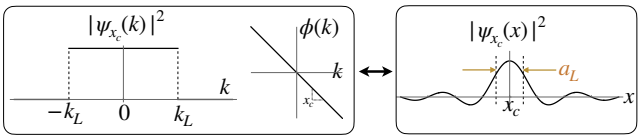

In summary, we find that although we cannot make a wavefunction localized to a point (Eq. 48), we can still make a "bump" at $x = x_c$, using the range of momenta in the lowest band. The form of $\psi_{x_c}(x)$ will recognized by anyone familiar with the diffraction-limited optics: a cylindrical lens creates an electric field at its foucus that has the same form. The first node in the diffraction-limited spot is at ♠.

A remarkable feature of $|x_c\rangle$ us that the displaced wave function is *orthogonal* to the original one at specific displacements:

$$\langle\psi_0|\psi_{\Delta x}\rangle = \left(\int_{-\pi/a_L}^{+\pi/a_L} dk'\, \langle k'|\right)\left(\int_{-\pi/a_L}^{+\pi/a_L} dk\, e^{-ik\Delta x}\, |k\rangle\right) = 2\frac{\sin(\pi\Delta x/a_L)}{\Delta x} \tag{54}$$

which is $= 0$ when $\Delta x = \pm a_L, \pm 2a_L, \pm 3a_L, \ldots$. So even though this function is only "approximately localized", and has amplitude beyond a single lattice site, the $|\psi_{x_c}\rangle$ at any one site is orthogonal to the $|\psi_{x_c'}\rangle$ at any other site.

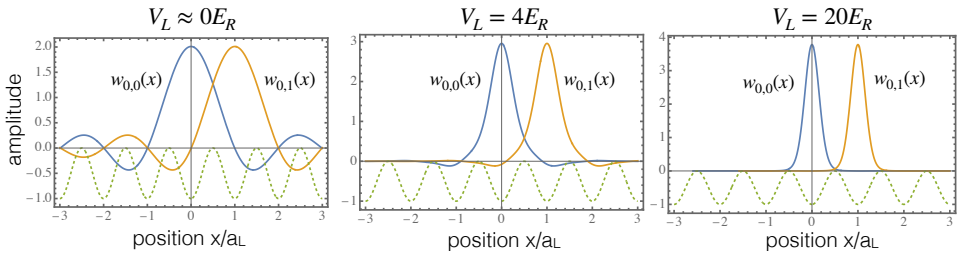

FIG. 6 **Wannier States of the lowest band.** Spatial representations of the Wannier states, Eq. 58, are shown here for lattice depths $V_L/E_R = 0, 4, 20$. The solid line shows $w_{0,0}(x)$ which (as discussed in the text) is has a functional form identical to all other $w_{0,j}(x)$, apart from a translation from $x = 0$ to $x = x_j = ja_L$. The yellow curves show $w_{0,j=1}(x)$, for example. The lattice potential is shown (dashed, offset, and with unity amplitude) for reference.

B. Wannier functions: a spatially localized basis

In a standing wave, certain positions are privileged: the locations at which the potential $V(x)$ is minimized, $x_j = a_L j$ (with integer j), which we will call the "locations" of the *lattice sites*. This is a fuzzy notion, since all quantum-mechanical wave functions are extended, or more precisely, localization is energetically expensive. In the limit $V_L \gg E_R$, the amplitudes of low-energy Bloch states are peaked around the $\{x_j\}$, as seen in §II.E.

At lattice sites, the idea of "diffraction limited localization" carries to a nonzero lattice, when using the Bloch basis instead of plane waves. Motivated by the discussion of the previous section, we define the *Wannier state* localized at $x = x_j = ja_L$ as

$$|w_j\rangle = \int_{-k_L}^{k_L} dq\, e^{-iqx_j} |q\rangle \tag{55}$$

where $|q\rangle$ is the Bloch state, and we consider only the lowest band for now. Applying the translation operator $\hat{T}_{a_L}$, Eq. 23, and using the defining characteristic of $|q\rangle$ that $\hat{T}_{a_L} |q\rangle = e^{-iqa_L} |q\rangle$, we find that

$$\hat{T}_{a_L} |w_j\rangle = |w_{j+1}\rangle \tag{56}$$

localized at $x = x_j - a_L$. Because of this, we can reference all Wannier functions to the $j = 0$ one, so that *each band has a unique Wannier function,* which we will call $|w\rangle$ (without reference to position). Including band indices explicitly, we have

$$\left|w^{(n)}\right\rangle = \int_{-k_L}^{k_L} dq\, |q, n\rangle \qquad \text{and} \qquad |w_{n,j}\rangle = \hat{T}_{x_j} \left|w^{(n)}\right\rangle \tag{57}$$

The spatial representation of the Wannier state is

$$w_{n,j}(x) = \langle x| \hat{T}_{x_j} \left|w^{(n)}\right\rangle = \langle x| \left(\int dx'\ |x'\rangle \langle x'|\right) \int_{-k_L}^{k_L} dq\, \hat{T}_{x_j} |q\rangle = \int_{-k_L}^{k_L} dq\, e^{-ix_j q} \Phi_{n,q}(x) \tag{58}$$

Examples of these are shown in Fig. 6. Again, note that $w_{n,j}(x) = w_{n,0}(x - x_j)$ so that there is a unique Wannier function for each band, copied at each lattice site. Because of this, we will sometimes drop the j index here too, and write $w^{(n)}(x)$. As mentioned above, one can show that there is a unique choice of the phases of Bloch states $\{\Phi_{n,q}(x)\}$ that results in Wanner functions that decay exponentially fast at infinity.[6] If our goal is to represent spatially localized particles, this is an important property! Two further properties may be useful: $w^{(n)}(x)$ are real, and have definite parity, i.e., $w^{(n)}(-x) = \pm w^{(n)}(x)$.

Like Bloch functions, the Wannier basis forms an orthonormal set:

$$\int dx\, w_{n,j}(x)\, w_{n',j'}(x) = \delta_{n,n'}\delta_{j,j'} \tag{59}$$

---

[6] For the sinusoidal potential we consider here, this choice is the same as was mentioned in §II.E: that $\Phi_{n,q}(x = 0)$ to be real and positive for even n, and $d\Phi_{n,q}(x)/dx|_{x=0}$ to be real and positive for odd n. (Kohn, 1959) can find such a choice for a lattice potential with mirror symmetry, and whose energy bands are disjoint.

(compare to Eqs. 46 and 47). The proof is left as an exercise (see App. C).

Notice that $|q\rangle$ and $|w_j\rangle$ are Fourier transform pairs. We can invert Eq. 55, such that

$$|q\rangle = \sum_j e^{iqx_j}\,|w_j\rangle \qquad \text{or} \qquad |q,n\rangle = \sum_j e^{iqx_j}\left|w_j^{(n)}\right\rangle \tag{60}$$

The key relation is

$$\boxed{\langle q|w_j\rangle = \exp(-iqx_j) \quad \text{and} \quad \langle w_j|q\rangle = \exp(iqx_j)} \tag{61}$$

This, along with inserting complete sets $\int dq\,|q\rangle\langle q|$ or $\sum |w_j\rangle\langle w_j|$, is the basis of all transformations between these two bases. Also, this reinforces the analogy to plane-wave states of the continuum, where $\langle k|x\rangle = \exp(-ikx)$.

It may bother you that we are replacing a continuum (of Bloch states across a range of q) by a discrete set (of Wannier states at each site). Are the number of states in these two bases the same? Some insight can be gained by putting the lattice in a box of length Ma_L. Here, M is the number of lattice sites, and a_L is the lattice period. Within this box, quasi-momentum become discretized

$$q = \frac{\pi}{Ma_L}\ell = k_L\frac{\ell}{M} \qquad \text{with} \quad \ell \in -M/2+1,\ldots,M/2 \tag{62}$$

with a maximum value $\pi/a_L = k_L$. The locations of lattice sites are $x_j = ja_L$, with j taking the range $-M/2+1,\ldots,M/2$ (or 0 to $M-1$, if preferred). In any case, we see that there are M discrete values of q_ℓ for quasi-momentum, which matches the number of sites x_j. For larger lattices, these both approach infinity at the same rate. Of course, this range of q covers only one Brillouin zone, and complete sets will also require a summation over bands, just like the Wannier states. Discretization has two further appeals: it simplifies units, and is also immediately amenable to numerical algorithms (which always require discretization). The continuum limit $\sum_q \to a_L\int dq/(2\pi)$ can always be taken.

C. Tunnelling

Returning to the question of atomic motion: how does a particle in "one place" – which we now know means, *initialized in a Wannier state at one lattice site* – evolves in time. In order to approach that problem, we will adopt the formalism of second quantization (App. B). This formalism is convenient since it lets us talk about single particles; more importantly, it lays the ground-work for a discussion of many particles in §VI, where particles interact, and where we will need particles to obey the correct exchange statistics.

We have already diagonalized the single-particle Hamiltonian. The total energy of a system the

$$E = \sum_{n,q} E_q^{(n)}\bar{N}_{n,q} \qquad \text{or} \qquad E = \sum_n \frac{a_L}{2\pi}\int_{-k_L}^{k_L} dq\,E_q^{(n)}\bar{N}_{n,q} \tag{63}$$

where $E_q^{(n)}$ are the eigenvalues of the (first quantized) Hamiltonian Eq. 20, and $\bar{N}_{n,q}$ is the number of particles at momentum q in the nth band. We are simply adding up the number of particles in each of these states. This total E is the expectation value of the many-body Hamiltonian

$$\hat{H} = \sum_n \frac{a_L}{2\pi}\int_{-k_L}^{k_L} dq\,E_q^{(n)}\hat{N}_{n,q} = \sum_n \frac{a_L}{2\pi}\int_{-k_L}^{k_L} dq\,E_q^{(n)}\hat{a}_{n,q}^\dagger\hat{a}_{n,q} \tag{64}$$

where $\hat{N} = \hat{a}^\dagger\hat{a}$ is the number operator, and $\hat{a}^\dagger$ and $\hat{a}$ are the creation and anihilation operators for particles. Here $\hat{N}_{n,q}$, $\hat{a}_{n,q}^\dagger$, and $\hat{a}_{n,q}$ are dimensionless. Notice a shift in perspective here: until now, by $\hat{H}$ we meant the Hamiltonian of a single particle; now, by $\hat{H}$ we mean the *total energy of a many-body system*, so that E is extensive.

Since $\hat{H}$ clearly breaks into bands, we can consider each band separately,

$$\hat{H} = \sum_n \hat{H}_{\text{band}}^{(n)} \qquad \text{with} \qquad \hat{H}_{\text{band}}^{(n)} = \frac{a_L}{2\pi}\int_{-k_L}^{k_L} dq\,E_q^{(n)}\hat{a}_q^\dagger\hat{a}_q \tag{65}$$

and often suppress the band index on $\hat{a}_q^\dagger$ and $\hat{a}_q$ for simplicity of notation, when discussing a single-band problem.

If $\hat{a}_q^\dagger$ creates a Bloch state, what is its relation to the operator that creates a Wannier state? Let's call it $\hat{b}_j^\dagger$, such that $|w_j\rangle = \hat{b}_j^\dagger |\text{vac}\rangle$. From Eq. 55, with $|q\rangle = \hat{a}_q^\dagger |\text{vac}\rangle$, we have

$$\hat{b}_j^\dagger |\text{vac}\rangle = \frac{a_L}{2\pi} \int_{-k_L}^{k_L} dq\, e^{-iqx_j} \hat{a}_q^\dagger |\text{vac}\rangle \tag{66}$$

These operators are thus Fourier Transform pairs. In discrete form, a symmetric representation is

$$\hat{b}_j^\dagger = \frac{1}{\sqrt{M}} \sum_q e^{-iqx_j} \hat{a}_q^\dagger \qquad \text{and} \qquad \hat{a}_q^\dagger = \frac{1}{\sqrt{M}} \sum_j e^{iqx_j} \hat{b}_j^\dagger \tag{67}$$

A spatially localized creation operator is the sum of all delocalized creation operators. Similarly, the creation of a particle in a single momentum state involves the (phased) creation of particles on all lattice sites. For the infinite lattice, we instead write these in a somewhat assymmetric way:

$$\hat{b}_j^\dagger = \frac{a_L}{2\pi} \int_{-k_L}^{k_L} dq\, e^{-iqx_j} \hat{a}_q^\dagger \qquad \text{and} \qquad \hat{a}_q^\dagger = \sum_j e^{iqx_j} \hat{b}_j^\dagger \tag{68}$$

In either case, the normalization factors are chosen such that any commutation relations between the $\hat{a}_q$ operators is preserved for the $\hat{b}_j$ operators, and vice versa.

We can now rewrite our Hamiltonian in terms of spatially local operators $\hat{b}_j$ and $\hat{b}_j^\dagger$.

$$\begin{aligned} \hat{H}_n &= \frac{a_L}{2\pi} \int_{-k_L}^{k_L} dq\, E_q \hat{a}_q^\dagger \hat{a}_q \\ &= \frac{a_L}{2\pi} \int_{-k_L}^{k_L} dq\, E_q \left(\sum_j e^{iqx_j} \hat{b}_j^\dagger \right) \left(\sum_{j'} e^{-iqx_{j'}} \hat{b}_{j'} \right) \\ &= \sum_{j,j'} \underbrace{\left(\frac{a_L}{2\pi} \int_{-\pi/a_L}^{\pi/a_L} dq\, E_q\, e^{iqa_L(j-j')} \right)}_{\equiv -t(\Delta j)} \hat{b}_j^\dagger \hat{b}_{j'} \end{aligned} \tag{69}$$

where $t(\Delta j)$ has units of energy, and depends only on $\Delta j = j - j'$. (We will justify the minus sign in its definition shortly.) In order to understand its meaning, consider the action of $\hat{b}_j^\dagger \hat{b}_{j'}$ for $j \neq j'$. This operator pair *anihiliates a particle at $x_{j'}$ and creates a particle at x_j*. This is what is meant by "hopping" from site j' to site j. For states whose energy is less than the lattice depth, such motion is classically forbidden: it is quantum-mechanical tunnelling.

The rate of tunnelling is related to the matrix element of $\hat{H}_n$ between two Wannier functions. We can see this by writing

$$\langle w_\ell | \hat{H}_n | w_{\ell'} \rangle = -\sum_{j,j'} t(j-j') \langle w_\ell | \hat{b}_j^\dagger \hat{b}_{j'} | w_{\ell'} \rangle = -t(\ell - \ell') \tag{70}$$

such that

$$-t(\ell - \ell') = \langle w_\ell | \left(\frac{\hat{p}_x^2}{2m} + V_L \sin^2(k_L \hat{x}) \right) | w_{\ell'} \rangle = \int dx\, w_\ell(x)^* \left(\frac{-\hbar^2}{2m} \frac{d^2}{dx^2} + V_L \sin^2(k_L x) \right) w_{\ell'}(x) \tag{71}$$

From this, and since $\hat{H}$ is hermetian, we can see that

$$t(-\Delta j) = t^*(\Delta j) \tag{72}$$

If the Wannier functions can be chosen to be real (see earlier discussion) then furthermore $t(-\Delta j) = t(\Delta j)$.

We do not need to use Eq. 71 to find the tunnelling coeffients. It is already evident in the dispersion relation for each band! From the definition of $t(\Delta j)$ in Eq. 69,

$$-t(\Delta j) = \frac{a_L}{2\pi} \int_{-\pi/a_L}^{\pi/a_L} dq\, E_q\, e^{iqa_L \Delta j} \tag{73}$$

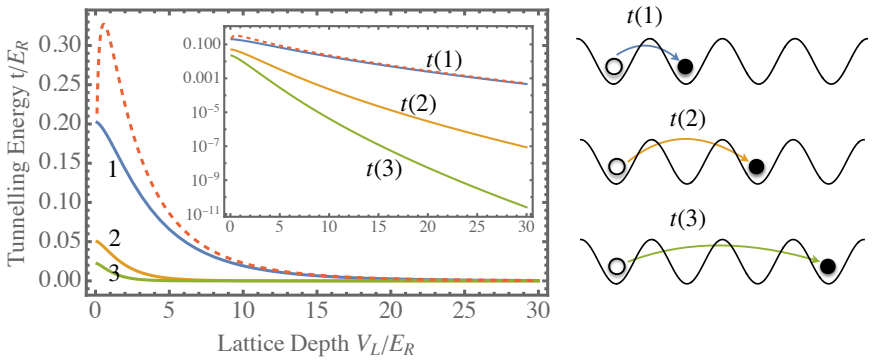

FIG. 7 **Tunnelling beyond nearest neighbour.** The tunnelling energies , calculated using Eq. 73, are shown as a function of lattice depth. The main figure shows a linear scale, and the inset shows the same data on a log scale. In principle, atoms can tunnel at infinitely long range. However the relative strength of any Δj greater than 1 is suppressed at a faster exponential rate than nearest-neighbour tunnelling. The dashed line is Eq. 77.

This is a conversion of E_q into a Fourier series. As we have discussed above, $E_q^{(n)}$ are periodic functions of q, with period $2\pi/a_L$, and have boundary conditions $dE/dq = 0$ at band edges; it is thus a cosine series:

$$E_q = \overline{E_q} - 2\sum_{\Delta j=1} t(\Delta j)\cos(a_L q \Delta j) \tag{74}$$

In sum, the dispersion relation $E_q^{(n)}$ for the nth band reveals the tunnelling rates between sites in real space.

D. The tight-binding limit

As an optical lattice becomes deeper, nearest-neighbour tunnelling becomes more and more dominant. We can see this in Fig. 7, where $t(1)$ $t(2)$, and $t(3)$ are shown for the lowest band, as a function of lattice depth. We see that $t(1)$ dominates, by a factor of 10 already at $V_L \approx 3E_R$, and by a factor of 100 at $V_L \approx 10E_R$.

In the limit where only $t(\Delta j)$ is significant, then we drop the Δj argument, such that the lowest-band energy is

$$E_q \approx \overline{E_q} - 2t\cos(a_L q) \qquad \text{“Tight-binding limit”, } t(2) \ll t(1) \tag{75}$$

Notice, looking at Fig. XX, that $E_q^{(0)}$ looks like an inverted cosine, with is minimum at $q = 0$, and thus $t > 0$ as defined here. As defined in Eq. 42, the band width is the difference between maximum and minimum energy. Thus

$$W_0 = 4t \qquad \text{(Tight binding)} \tag{76}$$

which is useful rule of thumb to remember.

In the deep-lattice limit, one can show (Campbell, 1955) that its tunnelling strength in the ground band is

$$t \approx \frac{W}{4} \approx \frac{4s^{3/4}}{\sqrt{\pi}}\exp\left(-2s^{1/2}\right)E_R \qquad \text{for } s \gg 1 \tag{77}$$

with $s = V_L/E_R$. The exponential decrease is characteristic of quantum tunnelling through a high barrier. This approximation is shown as a dashed line in Fig. 7.

In the tight-binding limit, one typically shifts zero energy to coincide with $\bar{E}_q^{(n=0)}$, and writes

$$\boxed{\hat{H}_{TB} = -t\sum_{<j,j'>}\hat{b}_{j'}^\dagger\hat{b}_j = -t\sum_j(\hat{b}_{j+1}^\dagger\hat{b}_j + \hat{b}_j^\dagger\hat{b}_{j+1}) = -t\sum_j\hat{b}_{j+1}^\dagger\hat{b}_j + \text{h.c.}} \tag{78}$$

where each of these forms is equivalent: $< j, j' >$ is a notation that means “neighbouring sites” (useful when going to higher dimensions or more complex geometries); and h.c. means “hermetian conjugate”.

Another insightful form of the TB hamiltonian comes from recognizing that $\hat{b}_{j+1}\hat{b}_j^\dagger$ is one-site discrete translation operator, which could also be written (back into first-quantized form) as $|w_{j+1}\rangle\langle w_j|$. In either case, we can then write the one-site translation operator as $\hat{T}_+ = \sum \hat{b}_{j+1}\hat{b}_j^\dagger$ or $\sum |w_{j+1}\rangle\langle w_j|$, which now acts on all sites. The TB Hamiltonian is then

$$\hat{H}_{TB} = -t(\hat{T}_+ + \hat{T}_+^\dagger) \tag{79}$$

Bloch states in the TB limit take a particularly simple form. The periodic $u(x)$ function is just the sum of all on-site Wannier functions, such that

$$|u\rangle = \sum_j |w_j\rangle \qquad \text{and} \qquad |q\rangle = \sum_j e^{iqa_L j}|w_j\rangle \qquad \text{(Tight binding)} \tag{80}$$

We can solve for the energy of this eigenstate with $\hat{H}_{TB}|q\rangle = E_q|q\rangle$, such that

$$E_q = -t(e^{iqa_L} + e^{-iqa_L}) = -2t\cos(a_L q) \qquad \text{(Tight binding)} \tag{81}$$

Thus we recover the single-cosine dispersion relation of Eq. 75.

E. Quantum Random Walks

If a single atom is initialized in a lattice site at x_j, what are the populations at later times? Let's write out a quantum "register" that has the occupations of the first five sites:

$$|\text{init}\rangle = |0\rangle_{-2}|0\rangle_{-1}|1\rangle_0|0\rangle_{+1}|0\rangle_{+2} \tag{82}$$

Applying the TB hamiltonian, Eq. 78, the particle can either hop to the left or hop to the right:

$$\hat{H}|\text{init}\rangle = -t|0\rangle_{-2}|1\rangle_{-1}|0\rangle_0|0\rangle_{+1}|0\rangle_{+2} - t|0\rangle_{-2}|0\rangle_{-1}|0\rangle_0|1\rangle_{+1}|0\rangle_{+2} \tag{83}$$

Taking one more discrete "step":

$$\hat{H}^2|\text{init}\rangle = -t^2|1\rangle_{-2}|0\rangle_{-1}|0\rangle_0|0\rangle_{+1}|0\rangle_{+2} + 2t^2|0\rangle_{-2}|0\rangle_{-1}|1\rangle_0|0\rangle_{+1}|0\rangle_{+2} - t^2|0\rangle_{-2}|0\rangle_{-1}|0\rangle_0|0\rangle_{+1}|1\rangle_{+2} \tag{84}$$

etc.

Remarkably, this experiment has been done. Fig. 8 shows a measurement of the time evolution of an atom in a single free direction, as a function of time (Preiss *et al.*, 2015). The occupations of sites are measured as a function of time. Atoms can be thought of as hopping from site to site with a characteristic time is $2\pi/t$.

IV. CURRENTS

We saw in the last section that a particle initialized in a single Wannier state will hop from site to site via tunnelling. Microscopically, movement of particles will alway rely on this process. However bulk transport of electrons through a crystal is not usually caused by initialization in a single Wannier state; rather, the movement of charge is induced by an electric field, whose force on particles induces a mass current. In this section, we will consider the speed at which non-equilibrium distributions move, and also find the equivalent of Newton's laws for particles in a lattice.

A. Currents and transport

For neutral particles, the analogue of electrical current is transport of mass. In free space, spatial velocity is related to the center-of-mass momentum by $v = p/m$. Things are not so simple in a lattice: as discussed in §II, momentum p and quasi-momentum q are not the same, such that $v \neq q/m$. Sometimes (such as in the first band), these two quantities do not even have the same sign! More generally, a single $|q\rangle$ state has multiple components with the same total momentum only if one includes the dressing by the photon field; however the momentum of photons is *not* associated with any mass-current. This makes the discussion of mass transport in optical lattices complex – and interesting!

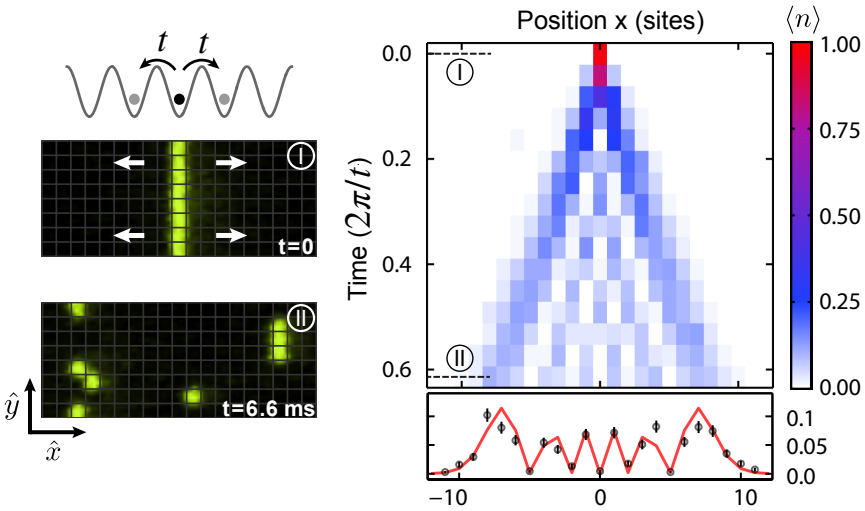

FIG. 8 **Tunnelling of a single particle.** In a two-dimensional optical lattice, particles are localized to a central column and restricted to tunnel only horizontally (along x, as labelled). Each atom undergoes a coherent quantum random walk; a single image collapses the wave function of each row, enabling a statistical measurement of occupations. (Preiss *et al.*, 2015)

We will define the total current as the particle number (N) times the velocity of the centre of mass (CM): $J = N v_{\rm CM}$, where

$$\hat{v}_{\rm CM} = \frac{i}{\hbar}[\hat{H}, \hat{X}_{\rm CM}] \qquad\qquad \hat{J} = \frac{iN}{\hbar}[\hat{H}, \hat{X}_{\rm CM}] \tag{85}$$

in which the CM position operator is

$$\hat{X}_{\rm CM} = \frac{1}{N}\sum_\ell x_\ell \hat{n}_\ell = \sum_\ell x_\ell \hat{b}_\ell^\dagger \hat{b}_\ell \,. \tag{86}$$

This definition of $\hat{J}$ gives the correct time dependence of expectation values, which we can see from the Ehrenfest Theorem,

$$\frac{d}{dt}\langle\hat{\mathcal{O}}\rangle = \frac{i}{\hbar}\langle[\hat{H}, \hat{\mathcal{O}}]\rangle + \langle\frac{\partial\hat{\mathcal{O}}}{\partial t}\rangle \tag{87}$$

applied to $\hat{\mathcal{O}} = \hat{X}_{CM}$.Since there is no explicit time dependence to $\hat{X}_{CM}$, we need only to calculate the commutator of $[\hat{H}, \hat{X}_{CM}]$.

$$\hat{J} = \frac{i}{\hbar}\sum_{\langle jk\rangle}\sum_\ell [t_{jk}\hat{b}_j^\dagger\hat{b}_k, x_\ell \hat{b}_\ell^\dagger \hat{b}_\ell] = \frac{i}{\hbar}\sum_{\langle jk\rangle} t_{jk}(x_k - x_j)\hat{b}_j^\dagger\hat{b}_k \tag{88}$$

where we have used $[\hat{b}_j^\dagger\hat{b}_k, \hat{b}_\ell^\dagger\hat{b}_\ell] = (\delta_{k,\ell} - \delta_{j,\ell})\hat{b}_j^\dagger\hat{b}_k$. For the general case, we can now use the site-indepenence of $t_{jk} = t(j-k) = t(k-j)$ and write a simpler form. We will here just write down the tight-binding limit,

$$\hat{J}_{\rm TB} = -\frac{ita_L}{\hbar}\sum_\ell(\hat{b}_\ell\hat{b}_{\ell+1}^\dagger - \hat{b}_{\ell+1}\hat{b}_\ell^\dagger) = -\frac{ta_L}{\hbar}\sum_\ell i\hat{b}_\ell\hat{b}_{\ell+1}^\dagger + \text{h.c.} \tag{89}$$

which has the units of $ta_L/\hbar$, a velocity. Notice that, apart from units, $\hat{J}$ has a form much like $\hat{H}_{\rm TB}$ itself, but with a minus sign between hopping terms. This means there must be an assymmetry between neighbouring site occupations for there to be a net current – which makes sense!

One also write down a *local* current operator, $\hat{j}_\ell = -i(ta_L/\hbar)\hat{b}_\ell\hat{b}_{\ell+1}^\dagger + \text{h.c.}$, which satisfies a continuity equation

$$\frac{d}{dt}\hat{n}_\ell + a_L^{-1}(\hat{j}_\ell - \hat{j}_\ell) = 0 \tag{90}$$

where $(d/dt)\hat{n}_\ell = (i/\hbar)[\hat{H}, n_\ell]$. This has the form of a typical continuity equation: the rate of change of local density is given by the spatial gradient of a current. If the current from the left and right are balanced, then the local density does not change. We will not work further with the local current in these notes, but instead consider the extensive transport that come from a global force.

B. Group velocity of a wave packet

The band structure energy diagrams we have derived, giving E_q, are also called "dispersion relations", which refers to the spatial dynamics of a wave packet. Let us consider a coherent superposition of Bloch states that are clustered about a central q_0 with a width of σ_q. A typical treatment considers a gaussian weighting, for example:

$$|\psi(t=0)\rangle = \sum f(q)\,|q\rangle \qquad \text{with} \quad f(q) = \exp\left[-(q-q_0)^2/\sigma_q^2\right] \tag{91}$$

Important for this discussion is that

$$\sigma_q \ll k_L \quad \text{such that} \quad \sigma_x \gg a_L \tag{92}$$

ie, this must be a delocalized wave packet. We can therefore expand the local energy about q_0:

$$E_q^{(n)} \approx E_q^{(n)} + (q-q_0)\left.\frac{dE_q^{(n)}}{dq}\right|_{q=q_0} + (q-q_0)^2\left.\frac{d^2E_q^{(n)}}{dq^2}\right|_{q=q_0} \tag{93}$$

We will find that each of these terms has a physical implication: the initial energy of $|\psi\rangle$, the velocity of its propagation, and its inertial response to an external force.

Let's first consider the spatial displacement of $|\psi\rangle$. It will be useful to define

$$v_g^{(n)}(q_0) = \frac{1}{\hbar}\left.\frac{dE_q^{(n)}}{dq}\right|_{q=q_0} \tag{94}$$

The time evolution of ψ is

$$\hat{U}\,|\psi(t=0)\rangle = \sum_q f(q)e^{i\hat{H}t/\hbar}\,|q\rangle = e^{-i\omega_0 t}\sum_q f(q)e^{iv_g qt}\,|q\rangle \tag{95}$$

where we have pulled out the common phase factor $\omega_0 = E_{q_0}/\hbar - q_0 v_g$. The remaining phase is equivalent to a discrete translation of each $|q\rangle$ state every $\tau = a_L/v_g$, which we can see by substituting $t = \tau\Delta j$ for integer Δj:

$$e^{iv_g qt}\,|q\rangle = e^{iv_g q\tau\Delta j}\,|q\rangle = e^{iqa_L\Delta j}\,|q\rangle = \hat{T}_{a_L\Delta j}\,|q\rangle \tag{96}$$

The time evolution of the wave packet is thus a pure translation at these intervals, plus a phase factor

$$|\psi(t=\tau\Delta j)\rangle = e^{-i\omega_0 t}\hat{T}_{a_L\Delta j}\,|\psi(t=0)\rangle \qquad \text{for} \quad \tau = a_L/v_g \tag{97}$$

Seen stroboscopically at these time intervals, $|\psi\rangle$ propagates at the group velocity v_g defined in Eq. . Note that a wave packet made in different bands will have a different v_g even if at the same quasi-momentum q_0.

So far, this discussion has been quite different in style from the discussion of $\hat{J}$ in §IV. Why is dE/dq related to current? Consider

$$\frac{dE_q}{dq} = \frac{d}{dq}\langle q|\,\hat{H}\,|q\rangle = \left(\frac{d}{dq}\langle q|\right)\hat{H}\,|q\rangle + \langle q|\,\hat{H}\left(\frac{d}{dq}\,|q\rangle\right) \tag{98}$$

where we have used the fact that $\hat{H}$ has no explicit dependence on q, and used a product rule. We can evaluate each derivative by inserting a complete set of Wannier states:

$$\frac{d}{dq}\,|q\rangle = \frac{d}{dq}\sum_j e^{ix_j q}\,|w_j\rangle = i\sum_j x_j e^{ix_j q}\,|w_j\rangle = i\sum_j x_j\,|w_j\rangle\,\langle w_j|q\rangle = iN\hat{X}_{CM}\hat{q} \tag{99}$$

where we have used Eq. 86. This gives us,

$$\frac{dE_q}{dq} = \left(-iN\,\langle q|\,\hat{X}_{CM}\right)\hat{H}\,|q\rangle + \langle q|\,\hat{H}\left(iN\hat{X}_{CM}\,|q\rangle\right) = iN\,\langle q|\,[\hat{H}, \hat{X}_{CM}]\,|q\rangle = \hbar\,\langle q|\,\hat{J}\,|q\rangle \tag{100}$$

Comparing to the definition of group velocity above, where E_q was the dispersion relation for a single particle, we have

$$v_g = \langle\hat{J}\rangle/N \tag{101}$$

C. External forces

Consider the modification of our original Hamiltonian Eq. 20 by the addition of an external force:

$$\hat{H}_F = \frac{\hat{p}^2}{2m} + V_L \sin^2(k_L \hat{x}) - F\hat{x} \tag{102}$$

This is no longer a translationally invariant hamiltonian, and thus Bloch states $|q\rangle$ are not longer eigenstates. Instead, for a weak force, one can show that the quasi-momentum of each Bloch state changes in time as

$$\frac{d}{dt}q(t) = \frac{1}{\hbar}F \tag{103}$$

In other words, *quasi-momentum changes linearly in time with an applied external force.* In this way, $\hbar q$ again behaves like free-space momentum p.

This problem was originally considered by Zener, who also found that if the force (or resultant $\dot{q}$) was too large, the problem became more complex: a particle that began in one band could end up in another one, due to non-adiabatic evolution of the quantum state, especially near small band gaps. Let's ignore this for now, and continue to work in the paradigm of a problem that can be broken into bands.

An intuitive picture for why $dq/dt = F/\hbar$ comes from considering the relative phase evolution of adjacent lattice sites. For a weak gradient, we can approximate the on-site Wannier functions as unchanged apart from a site-to-site phase evolution. For two quantum states shifted in energy by ΔE, their relative phase evolution is $\phi(t) = -(\Delta E)t/\hbar$, which in this case is $\phi(t) = Fa_L t/\hbar$. Across the entire lattice, we then have phases at x_j evolving as $\phi_j(t) = Fx_j t/\hbar$. The time dependence of a particular Bloch state is then

$$\hat{U}(t)\,|q\rangle = \sum_j e^{iqx_j}\hat{U}(t)\,|w_j\rangle = \sum_j e^{iqx_j}e^{iFx_j t/\hbar}\,|w_j\rangle = \sum_j e^{i(q+Ft/\hbar)x_j}\,|w_j\rangle = |q + Ft/\hbar\rangle \tag{104}$$

agreeing with Eq. 103.

In fact, this intuitive picture can be made more rigorous by considering the following unitary transformation of the problem:

$$\hat{U}_1(t) = \exp\{-i\hat{x}p_0(t)/\hbar\} \qquad \text{with} \quad p_0(t) = Ft \tag{105}$$

and we will also call $p_0(t) = -A(t)$, for reasons that become clear in a moment. In general, through a unitary transformation, the wave function is transformed to $\left|\widetilde{\psi}\right\rangle = U\,|\psi\rangle$, which obeys the Schrödinger equation under a new Hamiltonian,

$$\widetilde{H} = UHU^\dagger + i\hbar\frac{dU}{dt}U^\dagger \tag{106}$$

In our case

$$U_1\hat{x}U_1^\dagger = \hat{x}\,, \qquad U_1\hat{p}U_1^\dagger = \hat{p} + p_0(t)\,, \qquad i\hbar\frac{dU_1}{dt}U_1^\dagger = \hat{x}\frac{d}{dt}p_0(t) \tag{107}$$

such that

$$\begin{aligned} H_F \to \widetilde{H}_F &= \frac{(\hat{p} - A(t))^2}{2m} + V(\hat{x}) - F\hat{x} + \dot{p}_0\hat{x} \\ &= \frac{(\hat{p} + Ft)^2}{2m} + V(\hat{x}) \end{aligned} \tag{108}$$

Now that we have $\widetilde{H}_F$, we have recovered a periodic problem again. We can apply everything as we did before, for instance making use of Bloch functions, quasi momentum, etc. What do those eigenstates say about the solutions in our original frame of reference? We can, for instance, take $|\tilde{q}\rangle$ and transform it back to $|q\rangle$ using $U_1^\dagger$:

$$|q\rangle = U_1^\dagger\,|\tilde{q}\rangle = e^{+i\hat{x}p_0(t)/\hbar}\sum_j c_j\,|\tilde{q} + 2n\hbar k_L\rangle = \sum_j c_j\,|\tilde{q} + 2n\hbar k_L + p_0(t)\rangle = |\tilde{q} + p_0(t)\rangle = |\tilde{q} + Ft/\hbar\rangle \tag{109}$$

where we have used the fact that $e^{i\hat{x}p_0(t)/\hbar}$ is a *translation operator in momentum.* Since $\tilde{q}$ is time-independent in the transformed frame, we see that under $\hat{H}_F$, solutions are of the form $q_{\text{in}} + Ft/\hbar$. QED.

It's interesting to note that in the frame created by U_1, one can also write out a Tight-Binding Hamiltonian:

$$H_{F,TB} = -t\sum_j(\hat{b}^\dagger_{j+1}\hat{b}_j + \text{h.c.}) - F(t)\sum_j(ja_L)\hat{b}^\dagger_j\hat{b}_j \longleftrightarrow \widetilde{H}_{F,TB} = -t\sum_j(e^{ia_LA(t)/\hbar}\hat{b}^\dagger_{j+1}\hat{b}_j + \text{h.c.}) \tag{110}$$

where again, $A(t) = -Ft$ when the force is static. This looks like we've made a complex tunnelling strength,

$$t \longrightarrow te^{-ia_LFt/\hbar} = te^{-\phi(t)} \tag{111}$$

again following our intuitive picture that adjacent sites acquire a time-dependent phase in the presence of a force.

D. Effective mass

If an external force changes q, what current can it cause? We have already seen that $\hbar\dot{q} = F$ and $\hbar v_g = dE_q/dq$. Combining these,

$$\frac{dv_g}{dt} = \frac{dv_g}{dq}\frac{dq}{dt} = \frac{1}{\hbar}\frac{d^2E_q}{dq^2}\frac{dq}{dt} = \frac{1}{\hbar^2}\frac{d^2E_q}{dq^2}F \tag{112}$$

This gives us the lattice equivalent of "$F = ma$", which we will write $a = F/m$:

$$\frac{dv_g}{dt} = (m^*_q)^{-1}F \qquad \text{with} \quad \frac{1}{m^*_q} \equiv \frac{1}{\hbar^2}\frac{d^2E_q}{dq^2} \quad \text{(effective mass)} \tag{113}$$

We can best see the relationship between the second derivative of the dispersion relation and mass when considering a free particle: if $E = p^2/2m = \hbar^2q^2/2m$ (for zero lattice depth), then $m^* = m$ for all q. For deeper lattices, we can characterize the lowest band by m^*_0, the band curvature at $q = 0$. For tight banding, for instance,

$$(m^*_q)^{-1} = \frac{1}{\hbar^2}\frac{d^2}{dq^2}(-2t\cos qa_L) = \frac{2ta_L^2}{\hbar^2}\cos qa_L \qquad \text{such that} \qquad m^*_0 = \frac{\hbar^2}{2ta_L^2} \qquad \text{(tight binding)} \tag{114}$$

Note that one comes the same conclusion when finding $t(1)$ from Eq. 73 applied to a free-particle dispersion relation. The fact that t can be written proportionally to an inverse mass emphasizes the identification of tunnelling as a kinetic energy in the problem.

A strange thing about effective mass is that it does not need to be positive, or even finite. Since $m^*_q \sim 1/\cos(qa_L)$, it diverges at $qa_L = \pi/2$, halfway across the band, and comes to a value of $-m^*_0$ at the band edges. The dispersion relation at the band edges can be approximated as an *inverted parabola*, such that an interpretation as a "normal" massive particle breaks down. Perhaps a $q \approx \pm k_L/2$ things make a bit more sense: a small change in q (induced by an external F) will not change v_g here, because $v_g \sim \sin(qa_L)$ at its maximum there. See Fig. XX.

Finally, consider a thermal distribution of Bloch states, such as one would expect to find in equilibrium. We'll call this distribution f^{eq}. If an external impluse shifts the *entire distribution* by some $\Delta q = F\Delta t$, then a new distribution will deviate from the old one by

$$f^{\text{dev}}(q) = f^{\text{eq}}(q + \Delta q) - f^{\text{eq}}(q) \approx \frac{\partial f^{\text{eq}}}{\partial q}\Delta q \tag{115}$$

What current results? Notice that in equilibrium, there is no current, because $f(q) = f(-q)$, so an group velocity a that $|q|$ will cancel out. Thus

$$J = \int dq\, v_g f(q) = \int dq\, v_g f^{\text{dev}}(q) = \int dq\, v_g \frac{\partial f^{\text{eq}}}{\partial q}\Delta q \tag{116}$$

Using integration by parts, and the fact that $f^{\text{eq}}v_g = 0$ at the band edges, we can replace $v_g\partial f^{\text{eq}}/\partial q$ by $f^{\text{eq}}\partial v_g/\partial q$ under the integral. This gives,

$$J = \Delta q\int dq\, f^{\text{eq}}\frac{\partial v_g}{\partial q} = \Delta q\int dq\, f^{\text{eq}}\hbar\frac{1}{m^*_q} = \hbar\Delta q\left\langle\frac{1}{m^*_q}\right\rangle \tag{117}$$

where by $\langle 1/m^*_q\rangle$ we are indicating the *thermally averaged effective mass* across the band. When temperature is high enough that the occupation is equal everywhere in the band, then $\langle 1/m^*_q\rangle \to 0$, since any shift in q creates balanced positive and negative currents.

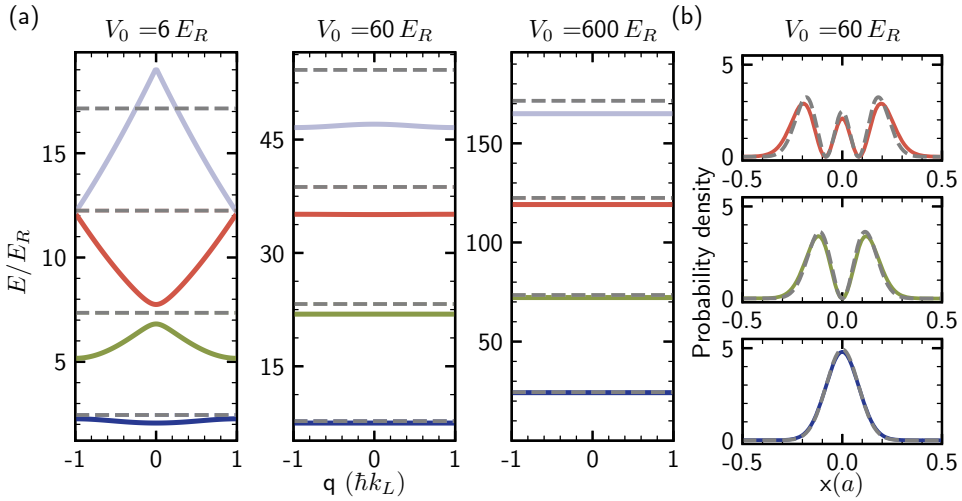

FIG. 9 **Deep-lattice limit.** (a) The band structure of a 1D optical lattice for depths of $6E_R$, $60E_R$ and $600E_R$. In each plot, $E^{(n)}(q)$ is shown for $n = 0$ (blue), $n = 1$ (green), $n = 2$ (red), and $n = 3$ (lavender). The dashed lines indicate the harmonic approximation of energy levels, $(n + \frac{1}{2})\hbar\omega_0$, which overestimate the lattice energy levels at all depths. (b) The on-site Wannier functions for the lowest three bands are shown at $V_L = 60E_R$. Here, the Wannier functions are well approximated by the harmonic-oscillator wavefunctions (dashed lines). [figure credit: V. Venu (Venu, 2022)]

V. THE ISOLATED-SITE LIMIT

For a sufficiently deep optical lattice, all tunnelling shuts down, and one is left with an array of isolated sites. A single particle in such a site experiences a harmonic oscillator potential (§V.A).

A. Harmonic approximation

When strongly confined in a single optical lattice site, the excursion of the atoms is much smaller than the lattice period: $k_L x \ll 1$. Because of this, we can expand the lattice potential:

$$V_L \sin^2(k_L x) \approx V_L (k_L x)^2 - \frac{1}{3} V_L (k_L x)^4 + \frac{2}{45} V_L (k_L x)^6 + \dots \tag{118}$$

The first term is simply a quadratic confinement. When comparing to $V_{\rm ho} = \frac{1}{2} m\omega_0^2 x^2$, we see that

$$\omega_0 = \sqrt{\frac{2V_L k_L^2}{m}} = 2\sqrt{V_L E_R} = 2\omega_R s^{1/2} \tag{119}$$

where $\omega_R = E_R/\hbar$ is the recoil energy in frequency units. and For ^{40}K in a 1064 nm lattice, $\omega_R = 2\pi \times 4.5\,$kHz; so the characteristic oscillation frequency is tens to hundreds of kHz.

The energy of a harmonic oscillator is

$$E_{\rm ho}^{(n)} = \omega_0 (n + \frac{1}{2}) \tag{120}$$

and becomes a reasonable prediction of $\bar{E}_q^{(n)}$, the average energy of each band. Figure 9 compares them.

Similarly, we know that the wave functions in a harmonic oscillator are given by Hermite polynomials. The final panel in Fig. 9 compares the Wannier states of the deep lattice to these. In particular, the ground state is

$$w^{(0)} \approx (\pi a_{\rm ho}^2)^{-1/4} \exp\left\{\frac{-x^2}{2a_{\rm ho}^2}\right\} \tag{121}$$

where the harmonic oscillator length is

$$a_{\rm ho} = \sqrt{\frac{\hbar}{m\omega_0}} = \left(\sqrt{\frac{\hbar^2}{2mE_R}}\right)^{1/2} s^{-1/4} = \frac{a_L}{\pi s^{1/4}} \tag{122}$$

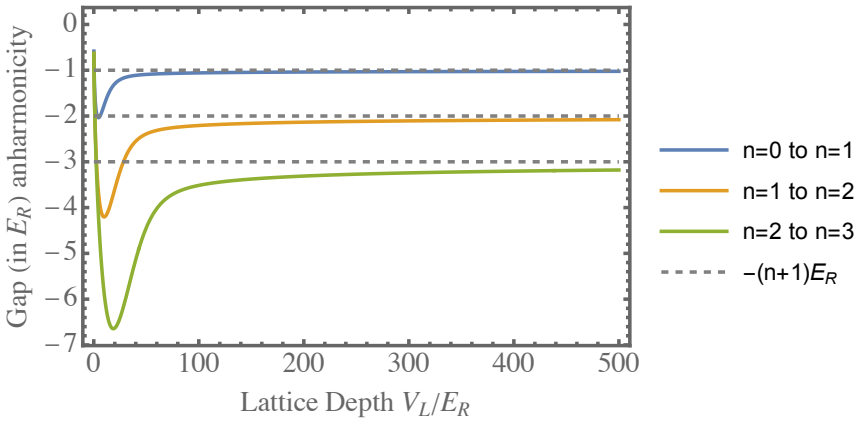

FIG. 10 **Anharmonicity.** The difference between the expected energy gap, $\hbar\omega_0$, and the actual band gap is shown versus lattice depth. We find that even in the deep-lattice limit, a remnant anharmonicity of $-(n+1)E_R$ remains, shown as dashed lines.

We see that self-consistency of the original approximation, $k_L x \ll 1$, requires that $s^{1/4} \gg 1$.

This leaves us with a characteristic hierarchy of energy and length scales:

$$E_R \ll \{\hbar\omega_0 \approx \mathrm{BG}\} \ll V_L \qquad \text{and} \qquad a_L \gg a_{\mathrm{ho}} \tag{123}$$

We can also use this to estimate the number of bound states in a deep lattice. If the spacing is $\hbar\omega_0$, then

$$\text{number of deeply bound states} \approx \frac{V_L}{\hbar\omega_0} = \frac{sE_R}{2E_R s^{1/2}} = \frac{1}{2}s^{1/2} \tag{124}$$

where we have neglected the zero-point energy. Looking back at Fig. 5, we can see that as V_L exceeds the energy of a particular energy range, the gaps are perhaps larger, but it would not be evident from the band structure, a priori, which energies were "trapped". Perhaps the $E_q^{(n)} < V_L$ vs. $E_q^{(n)} > V_L$ distinction is instead that particles with energies above the lattice depth can move classically between sites; whereas those with energies below must tunnel. The appearance of gaps above V_L reminds us that quantum reflection can occur even for purely attractive potentials. In this case, we have already outlined how the Bragg scattering an every integer multiple of $\hbar k_L$ is a polynomial function of V_L (see Eq. 38).

Anharmonicity of sinusoidal confinement provides the first deviation from the predictions laid out above. Through perturbation theory, one finds

$$\begin{aligned} V_{\mathrm{OL}}^{(n)} \equiv \langle n|\, V_L \sin^2(k_L x)\, |n\rangle &= V_L k_L^2 \langle n|\, x^2\, |n\rangle - \frac{1}{3}V_L k_L^4 \langle n|\, x^4\, |n\rangle + \frac{2}{45}V_L k_L^6 \langle n|\, x^6\, |n\rangle + \dots \\ &= \underbrace{2\sqrt{E_R V_L}(n+1/2)}_{\text{harmonic}} \underbrace{- E_R\left(\frac{2n(n+1)+1}{4}\right)}_{\text{ind. of } V_L} - \mathcal{O}\left(\sqrt{\frac{E_R^2}{V_L}}n^3\right) \end{aligned} \tag{125}$$

We can then see that the band gap between two successive bands is, neglecting terms that fall off as $V_L^{-1/2}$ or faster,

$$V_{\mathrm{OL}}^{(n+1)} - V_{\mathrm{OL}}^{(n)} \approx \hbar\omega_0 - (n+1)E_R \tag{126}$$

such that it is always less than $\hbar\omega_0$. A comparison is shown in Fig. 10.

B. Higher bands

Fig. 11 shows the width of the lowest bands versus lattice depth. We see that eventually the lowest band becomes *flat*: this means that tunnelling is insignificant. However, even after the ground band is "frozen out", the first excited band may still be active: see Fig. 11.